KU LEUVEN

FACULTEIT WETENSCHAPPEN

# Lattice location of Mn in GaAs and GaN

**Arnaud De Coster**



Promotor: Prof. L.M.C.Pereira
Co-promotor: *K. Temst*
Co-promotor: *A. Vantomme*

Proefschrift ingediend tot het
behalen van de graad van
Master of Science in Physics

Academiejaar 2014-2015

# Acknowledgement

*"To envision us coming up and pounding on this door, pounding and pounding, not just wanting admission but needing it, we don't know what it is but we can feel it, this total desperation to enter, pounding and pushing and kicking, etc. That, finally, the door opens...and it opens outward: we've been inside what we wanted all along. Das ist komisch."*

*David Foster Wallace*

"It's not about the destination but about the journey". While too trite a quote to place above this acknowledgement, trite tends to hold true and it certainly holds for this thesis. Among the many people who helped me out along the way of this journey I want to first sincerely thank Professor Pereira for introducing me to the topic and emission channeling. Your comments and guidance were invaluable not only for the thesis but for what it means to be a scientist in general.

Except in the literal sense, science never happens in a vacuum, I was blessed to be surrounded by many helpful people at IKS and during the beamtime at ISOLDE. Thank you professor Wahl and doctor Correia for giving me a taste of the gritty work that lies behind the pretty pictures of emission channeling, my experience at CERN was unforgettable. Many thanks go to Tiago and Valerie for answering my incessant questions and the support for when the inevitable doubts came about the completion of this work. Daily life at IKS was made so much sweeter thanks to the tea and coffee breaks with my other office mates as well, Hiwa and Enric, thank you for making the respite of thesis work so pleasant. Lastly, I'd like to thank Daniel, Nuno, Koen, Sergio and many others for helping me in the lab or with puzzling results.

Reaching the end of my master would not have been possible if it weren't for the many friendships I got to make during my studies and Erasmus. Taking the risk of singling out anyone in particular: Bram and Ruben, you were the best room mates and friends I could've asked for in the past few years.

Finally, my family and parents for their unconditional love and support.

# Samenvatting

Het onderzoeksveld van verdund magnetische halfgeleiders(VMH) heeft in de voorbije deccenia veel ontwikkeling doorgemaakt, zowel vanuit een fundamentele interesse in de link tussen de magnetische en geleidende eigenschappen als de potentiële toepassingen in computer technologie. Hoewel het voorkomen van zowel halfgeleidende als magnetische eigenschappen in een materiaal op zichzelf niet bijzonder is, zijn de VMH uitzonderlijk omdat het de ladingsdragers zijn die mediëren tussen de magnetische momenten in het rooster en zo de ferromagnetische ordering veroorzaken. Zowel het magnetische moment als de ladingsdragers worden geleverd door transitie-metalen (TM), gedoteerd in een klassieke halfgeleider. De locatie waar het TM wordt opgenomen in het kristal bepaalt of het zich zal gedragen als acceptor of donor en hoe het koppelt aan andere magnetische momenten. Om een beter begrip te krijgen van deze materialen is dus accurate kennis over de locatie die het TM opneemt in het kristal noodzakelijk. In deze thesis wordt de rooster locatie van Mn in GaAs and GaN bestudeerd, twee model-materialen uit respectievelijk de kleine- en grote-bandkloof VMH.

Voor Mn geïmplanteerd GaAs, meer compact neergeschreven als (Ga,Mn)As is het ferromagnetisch gedrag relatief goed begrepen in de context van het ladingsdrager gemedieerde mechanisme eerder beschreven dat het magnetische moment van substitutionele Mn atomen oplijnt. Afgezien van substitutioneel Mn ($Mn_{Ga}$) is er ook interstitieel Mn ($Mn_{int}$) aanwezig, waarvan bekend is dat het een donor is. Dit compenseert de positieve holtes bijgedragen door $Mn_{Ga}$ en koppelt hier bovendien ook nog anti-ferromagnetisch mee. Gebruik makende van de techniek van emissie-kanalisatie (EK) werd de roosterlocatie van $Mn_{int}$ in een dunne (Ga,Mn)As film van 4% onzuiverheid concentratie verkregen door ionen implantatie gevolgd door gepulseerde laser smelting (II-PLS), bepaald. De gevonden locatie is de $T_{As}$ site, met tetrahedrale symmetrie en gecoördineerd door 4 As atomen. De thermische stabiliteit werd ook bestudeerd door de fracties van Mn aanwezig te meten na verschillende stappen van opwarming. Voor de diffusie van $Mn_{Ga}$ werd een activatie energie ($E_a$) van 2.1 eV gevonden. Eerdere resultaten met (Ga,Mn)As films geproduceerd met moleculaire straal epitaxie (MSE) van 1% and 5% onzuiverheids conncentratie vonden respectievelijk een activatie energie die groter en kleiner was dan

voor het II-PLS film. Wij suggereren dat de diffusie van substitutioneel Mn een effect is dat voornamelijk afhangt van de concentratie en best geïnterpreteerd kan worden in de context van een gaten-uitwisselings mechanisme in een percolatie cluster van Mn atomen. Voor interstitieel Mn werd een een activatie energie van 0.9-1.2 eV bepaald. Deze waarde is beduidend lager dan de activatie energie van de eerder vernoemde MSE films. Dat $Mn_{int}$ een dergelijke lage thermische stabiliteit bezit wordt toegeschreven aan de aanwezigheid van een intern elektrisch veld dat de diffusiviteit verbetert. Dit elektrisch veld wordt beschouwd als een gevolg van een niet-uniforme ladingsdrager verdeling, veroorzaakt door het profiel van elektrisch actief $Mn_{sub}$ in het II-PLS film.

Hoewel in GaN algemeen wordt geaccepteerd dat Mn substitueert voor het cation zijn er ook experimentele resultaten van kleinere hoeveelheden anion substitutie. Aangezien deze anion fractie zowel de elektrische als magnetische eigenschappen kunnen beïnvloeden door als compenserend defect op te treden, is het van belang om te bepalen of deze anion fractie al dan niet aanwezig is. Op basis van eerdere EK experimenten is ook een selectie mechanisme voor deze anion substitutitie voorgesteld afhankelijk van de locatie van het Fermi-niveau. Om deze hypothese te testen werd de locatie van Mn geïmplanteerd (Ga,Mn)N, p-type GaN and n-type GaN bepaald met EK. Voor alle drie de films werd de locatie bepaald als $Mn_{Ga}$ en $Mn_{Ga}$ verplaatst naar de $AB_{Ga}$ site. Deze verplaatste fractie wordt toegeschreven aan de formatie van een defect complex met stikstof gaten, gevormd gedurende de implantatie. Er werd geen kwalitatief verschil in de verplaatsing vastgesteld tussen de gedopeerde GaN films, wat niet verwacht werd op basis van de locatie van het Fermi-niveau. Onze aanname is dat dit het gevolg is van Fermi-niveau vastzetting door de hoge concentratie van defecten gevormd gedurende de implantatie.

# Summary

The field of dilute magnetic semiconductors (DMS) has seen a lot of development in the past decades, both from a fundamental interest in the linkage of magnetic and conducting properties and with an eye to potential applications in computer technology. While the presence of semiconducting properties and magnetism in a given material is not out of the ordinary, DMS materials stand out because the charge carriers actually mediate between magnetic moments in the lattice, causing the ferromagnetic ordering. These magnetic moments and charge carriers are supplied by transition-metal (TM) dopants in a classic semiconductor. The location where these dopants are incorporated will determine if they will act as either an acceptor or donor and how they will couple to other magnetic moments. Hence, in order to achieve a better understanding of DMS, accurate knowledge of the lattice location the TM takes up in the crystal is vital. In this thesis the lattice location of Mn in GaAs and GaN is studied, two model materials from respectively the narrow-gap and wide-gap DMS families.

For Mn implanted GaAs, written more compactly as (Ga,Mn)As, the ferromagnetic behaviour is relatively well understood by the charge-carrier mediated mechanism described above, which aligns the substitutional Mn magnetic moments. Aside from substitutional Mn ($Mn_{Ga}$) also interstitial Mn ($Mn_{int}$) can be present which is known to be a donor, compensating the hole charge carriers offered by the substitutional Mn acceptors. Moreover it couples anti-ferromagnetically to $Mn_{Ga}$ reducing the ferromagnetism. Using the technique of emission channeling (EC) the lattice location of $Mn_{int}$ in a (Ga,Mn)As thin film at 4% impurity concentration prepared by ion implantation and pulsed laser melting (II-PLM) was determined to be the $T_{As}$ site. The thermal stability was studied as well by considering the fractions of Mn present after different annealing steps. For diffusion of substitutional Mn an activation energy ($E_a$) of 2.1 eV was found. Previous findings on (Ga,Mn)As thin films prepared by molecular beam epitaxy (MBE) of 1% and 5% impurity concentration found an activation energy respectively higher and lower than for the II-PLM sample. We suggest that the diffusion of substitutional Mn is an effect dependent mainly on the concentration and is best interpreted in terms of vacancy-assisted diffusion in a percolation cluster of Mn atoms. For interstitial Mn $E_a$ was determined to be 0.9-1.2

eV. This value is much lower than the activation energy found in the aforementioned MBE samples. That $Mn_{int}$ has a significantly lower thermal stability in the II-PLM film compared to the MBE films is interpreted as a consequence of the presence of an internal electric field, enhancing the diffusivity of $Mn_{int}$. The electric field is assumed to be generated by a non-uniform charge carrier distribution, resulting of the depth profile of electrically active $Mn_{sub}$ in the II-PLM film.

Although in GaN cation substitution by Mn is accepted there have also been reports of minority anion substitution. Since this anion fraction ($Mn_N$) may affect the electrical and magnetic properties by acting as a compensating defect (similar to $Mn_{int}$ in (Ga,Mn)As), it is important to determine whether or not is it present, and if so, in which number. On basis of earlier EC experiments also a selection mechanism for anion substitution to take place, depending on the location of the Fermi-level in the band-gap, had been proposed. To test this hypothesis the lattice location of Mn implanted (Ga,Mn)N, p-type GaN and n-type GaN was determined with EC. For all three samples the $Mn_{Ga}$ and $Mn_{Ga}$ displaced towards the $AB_{Ga}$ site were found. This displaced fraction is attributed to the formation of a defect complex with nitrogen vacancies created during implantation. No qualitative difference in displacement is found between the doped GaN samples, contrary to what is expected on basis of the location of the Fermi-level. We assume this is due to implantation damage causing the Fermi-level to be pinned in the middle of the bandgap, locally negating the effect of the dopants.

# Vulgariserende samenvatting

Het huidige leven in de westerse wereld is bijna ondenkbaar zonder computer technologie. In vergelijking met de eerste gigantische machines die hele kamers konden vullen zijn onze huidige computers geminiaturiseerd tot nog maar het formaat van je broekzak. Deze razendsnelle ontwikkeling staat bekend als de 'wet' van Moore, die stelt dat de rekencapaciteit van een processor elke 18 maanden verdubbelt. Continue schaalverkleining is echter onmogelijk, eenmaal op de schaal van individuele atomen worden kwantum effecten belangrijk die de eigenschappen van de transistor verslechteren.

De zogenaamde verdund magnetische halfgeleiders (VMH) zijn één mogelijke optie om het breken van de 'wet' van Moore nog even af te houden. Deze materialen combineren de geleidende eigenschappen van de klassieke halfgeleider die gebruikt wordt in transistoren, en de magnetische eigenschappen van de metalen die tegenwoordig worden gebruikt in harde schijven. Helaas zijn de temperaturen waarbij het magnetisme aanwezig is, nog ver onder kamertemperatuur en dus zijn zelfs de beste VMH nog niet te gebruiken voor toepassingen in het dagelijkse leven. Een van de redenen dat het verhogen van de gebruikstemperatuur zo moeilijk blijkt te zijn is het gebrek aan theoretisch en experimenteel begrip van deze materialen. Tijdens de groei van een VMH worden magnetische atomen geïntroduceerd in het kristalrooster van een halfgeleider. Echter is het nog niet volledig duidelijk welke positie ze exact gaan nemen in het rooster, noch is het volledig begrepen hoe deze atomen zich zullen verplaatsen -het diffusie-gedrag- bij het opwarmen van het kristal. In deze thesis werd de locatie en de diffusie van mangaan atomen bestudeerd in de halfgeleiders gallium arsenide en galliumnitride.

Met behulp van de techniek van emissie kanalisatie, uitgevoerd in ISOLDE aan het CERN werd gevonden dat Mn in gallium arsenide twee locaties bezet, de substitutie van de gallium positie enerzijds en de interstitiële positie, tussen 4 arsenide atomen anderzijds. Bij het opwarmen van het kristal bleek dat de diffusie van het substitutionele mangaan op een eenduidige manier afhing van de concentratie van mangaan in de VMH, namelijk dat bij hogere concentratie substitutioneel mangaan bij lagere temperaturen difusseert. Voor interstitieel mangaan blijkt er geen eenduidig verband te zijn met de concentratie in-

dien twee gallium arsenide kristallen, op andere wijze vervaardigd maar met gelijkaardige concentratie, worden vergeleken. Dit werd geinterpreteerd als het gevolg van een intern elektrisch veld dat de diffusie van mangaan verbeterd. Omdat de magnetische eigenschappen verstoord worden door de aanwezigheid van het interstitieel mangaan is begrip van het diffusiegedrag uiterst belangrijk voor het ontwikkelen van methodes om dit te verwijderen uit het kristal zonder diffusie van substitutioneel mangaan te veroorzaken. Dit onderzoek biedt een van de puzzelstukken om dit te bewerkstelligen. Ook werd de locatie van mangaan in gallium nitride bestudeerd. Er werd vastgesteld dat mangaan hier een combinatie van substitutie met gallium en licht verplaatst van de substitutie met gallium bezet. Dit werd geïntepreteerd als het gevolg van de interactie met stikstof defecten in het rooster, gevormd tijdens de implantatie van de bestudeerde mangaan atomen.

# Contents

# Chapter 1

# Introduction

## 1.1 Motivation

In this day and age, one would be hard pressed to find someone in our (western) world whose life isn't shaped by computer technology, whether it is at the workplace or at home, in the form of PC's or smart-phones. It is difficult to imagine that only sixty years ago computers were still a curiosity, only to be found in university labs or military bases. Although in any revolution pinpointing the exact moment it started is impossible, one can single out the invention of the bipolar transistor in 1947 and the integrated circuit in 1958 as watershed moments in the computer revolution. Both devices were based on semiconductor technology, which has seen continuous development and refinement up to this day. This is of course ever in the pursuit of higher efficiencies, computing power and fear of the dreaded violation of Moore's law. So far this 'law' has held up, with experts claiming the earliest date for its demise as 2020. The reason being, of course, the fundamental physical limits placed on conventional silicon semiconductor technology as the length scale of a single transistor decreases.

One possible solution to circumvent this limit would be to step outside the conventional electron or charge transport paradigm and incorporate the spin degree of freedom of the electron. Manipulation of both the electron spin and charge would directly lead to more information transport and processing power and is the basis of the field of *spintronics*.[1] The very first investigations by Mott revealed that at low temperatures majority and minority spin electrons do not mix during scattering in a ferromagnet.[2] The conductivity is then expressed as the sum of two, oppositely spin polarised currents. This two-current model eventually led, with some modifications, to the discovery of the giant magnetoresistance (GMR) effect in 1988.[3] This effect shows itself when a current passes through

a thin layer structure of a ferromagnet, non-ferromagnet and a ferromagnet. Depending on whether the magnetisation of the ferromagnets are parallel or anti-parallel to each other the two spin-polarised currents scatter differently, leading to a different resistance. Since the magnetisation of the thin layer can be controlled by an external magnetic field this makes it possible to manipulate the conductivity. GMR and later the similar tunneling magneto-resistance (TMR) effect were the first real-world spintronics applications in the form of spin-valves, being used in the reader heads of hard-drives.[4]

Although the discovery of the GMR and subsequently TMR effect quickly led to an immediate technological impact (as demonstrated by the award of the 2007 nobel prize for GMR) in the field of data storage, it did not affect integrated circuit technology. Essentially this is due to the incompatible metal-based data storage technology and semiconductor-based processing of the data as well as the incompatible crystal structures.[5] Because of this the goal of spintronics shifted towards an integration of both in dilute magnetic semiconductors (DMS). Although magnetic semiconductors -which incorporate rare-earth or transition metals in the chemical formula- are common, they are incompatible with current semiconductor technology based on Si, GaAs and Ge. Current research is then focussed on developing room-temperature magnetic semiconductors by doping classical semiconductors with magnetic elements. Several proof of concept devices already exist such as spin field-effect transistors and spin diodes but commercialisation is still far off in the future as long as room-temperature ferromagnetism is not realised. [4]

## 1.2 History of DMS

The first generation of DMS developed and studied were of the form $A^{II}_{1-x}Mn_xB^{VI}$ during the 80's.[6] By doping the II-VI semiconductor host (such as CdTe, ZnSe) with $Mn^{2+}$ which has the same valence as the II-cation of the host, several novel magnetic effects could be observed such as giant Faraday rotation and large Zeeman splitting of the electronic levels.[7] However their interesting spin effects manifest only at very low temperatures and these materials are dominated by an anti-ferromagnetic interaction making them unlikely candidates for practical applications.

The development of the non-equilibrium low temperature molecular beam epitaxy (LT-MBE) technique allowed researchers to overcome the low solubility of transition metals in III-V semiconductors. These materials are already widely used in the electronics and semiconductor industry and are interesting both for the wealth of knowledge and know-

how already available and possible future integration. In 1989 Munekata et al. synthesised (InMn)As and found ferromagnetic order up to a temperature of 7.5 K using LT-MBE.[8] This was followed up by the growth of GaMnAs in 1996 with a curie temperature of 60 K.[9] The great advantage of doping III-V semiconductors with $Mn^{2+}$ is the large amount of free holes available which mediate the ferromagnetic interaction. Since its discovery GaMnAs has become the canonical DMS, used in proof-of-concept devices and capable of the highest Curie temperatures ($\approx$ 190 K)[10]. Further increases in temperature have proven difficult, partly due to a lack of understanding of the exact mechanism at play in III-V DMS.

Around the beginning of the 21st century a new class of DMS based on wide-gap semiconductors and oxides were predicted to be ferromagnetic at room temperature.[11] Very soon afterwards experimental confirmation was found in materials such as Mn doped GaN and ZnO, or (Ga,Mn)N and (Zn,Mn)O, leading to a flurry of activity and interest in the field. However reproducibility proved difficult with issues of contamination, formation of precipitates and measurement artefacts. Moreover, carefully characterised samples only showed paramagnetism, anti-ferromagnetism or at best ferromagnetism up to 10 K.[12][13][14]

That leaves us at the present day, with research currently divided between narrow-gap DMS and wide-gap DMS. Narrow-gap semiconductors such as (Ga,Mn)As and (In,Mn)As have widely been shown to exhibit carrier-mediated ferromagnetism and have already shown their use in possible devices. However their Curie temperature is still much below room temperature and the exact mechanism leading to the ferromagnetic state is still not fully understood. Wide-gap semiconductors on the other hand seem elusive in understanding the origin of their claimed ferromagnetism at room temperature and experimental confirmation. In the following section we will look more in depth at the theoretical basis, and experimental knowledge acquired of both narrow- and wide-gap DSM in general and GaN and GaMnAs in particular.

## 1.3 GaMnAs

### 1.3.1 Ferromagnetism and models

The III-V dilute magnetic semiconductor (Ga,Mn)As which crystallises in the zincblende structure is the archetypal example of a DMS material and is the perfect system to study the effect of the lattice location of the TM on its magnetic properties, both with hopes of improving its curie temperature but also from a theoretical viewpoint. When GaAs is

doped with Mn, the majority of Mn will substitute for Ga. Mn has the following electron structure $[Ar]3d^5 4s^2$ and in the gallium site ($Mn_{Ga}$) is incorporated in the 2+ charge state. Since GaAs is a III-V semiconductor, $Mn_{Ga}$ will have a $3d^5$ valence electron structure offering an itinerant hole and a localised magnetic moment (S=5/2). At concentrations of a few percent and up, which are typical for high $T_c$ (Ga,Mn)As films, a minority fraction of Mn will occupy interstitial positions, i.e. a non-substitutional lattice location. As shown both theoretically and experimentally, interstitial Mn is a double donor, reducing the hole concentration and coupling anti-ferromagnetically to the substitutional $Mn_{Ga}$. Hence it has a twofold compensating effect, first it reduces the amount of Mn contributing to magnetic order as $x_{eff} = x_{sub} - x_i$ with $x_{sub}$ and $x_i$ being the fractions of substitutional and interstitial manganese respectively. And secondly it reduces the hole concentration given by $p = 4\frac{x_{sub}-x_i}{a^3}$ where a is the lattice constant. [15] [16]

From the effects on hole concentration and magnetic moments it is obvious that $Mn_{Ga}$ plays an important role in determining the curie temperature and magnetisation. The precise dependence on the interstitial concentration is still under debate with two models being put forward to describe (Ga,Mn)As. The first one, proposed by Dietl. et al. in 2000 is based on the mean field p-d zener model. In the framework of this model the band carriers promote ferromagnetic ordering between the localised (d-shell) spins by a lowering of their energy. This lowering is effected by a redistribution between the spin sub-bands split by the exchange coupling between the sp carrier spins and the d shell localised spins.[17] However a more detailed quantum mechanical treatment showed that the interaction between magnetic moments oscillates with the distance between them according to the famous RKKY formula. It has however been shown that in a mean field, continuous medium approximation, these models are equivalent. This corresponds to the situation when the RKKY oscillation $\frac{\pi}{k_f}$ is large compared to the localised spin distance. In the case of DMS the mean field Zener model is then applied since it is technically simpler and leads to the same results. Despite not taking into account many other effects such as thermodynamical fluctuations, anti-ferromagnetic interactions between $Mn_{Ga}$ and disorder except on a phenomenological level, it still offers qualitative and often also quantitative estimates of $T_c$ in DMS.[17][18] It is also argued that the p-d zener model applies on the insulator side of the MIT (metal-insulator transition). From the scaling theory of the Anderson-Mott transition it follows that the average hole localisation length, which diverges at the MIT, remains much larger than the mean acceptor distance over the experimentally important hole density range. Hence the model can also serve to estimate $T_c$ on the insulator side of the MIT transition with the caveat of weak hole localisation. Experimental confirmation came by the evaluation of the $Mn_{sub}$ exchange energy in ZnMnTe[19] showing the expected value despite being on the insulator side of MIT.

A different model, fundamentally opposing the p-d Zener model is the impurity band model. In contrast with the p-d Zener model where the carriers and d acceptor states both remain in the valence band, the impurity band model posits that states derived from the impurity d-states are located in the band gap, the relevant spin-spin coupling being the double exchange. This model was a result of ab-initio calculations [20][21] and backed up by a series of magneto-optical, transport and magnetisation measurements, for example by Dobrowolska et al. in 2012.[16] They showed that contrary to the p-d Zener model prediction, $T_c$ did not depend monotonically on the hole concentration, instead being determined by the location of the Fermi-level in the impurity band. In the middle of the band lie the extended states with the highest density of states (DOS). Metallic samples which have their Fermi level here have the highest $T_c$. Conversely, if the Fermi level is located at the tails of the the impurity band, DOS is low and the states are localised leading to insulating samples with low $T_c$. The location of the Fermi-level is determined by the concentration of the interstitial manganese as can be seen by considering the filling factor of the impurity band: $f = \frac{x_{sub}-2x_i}{x_{eff}}$. This then implies that instead of eliminating interstitial manganese to reach high $T_c$ as the p-d Zener model suggests, interstitial manganese can actually aid the ferromagnetic ordering.

It is clear from the discussion of the two models presented here that an adequate understanding of the mechanism behind the ferromagnetism in GaMnAs is crucial in the quest for higher Curie temperatures. This is already obvious in the most basic question of whether or not to eliminate interstitial manganese in post-growth processing. In the end reality is probably too subtle to be described by one single model. As pointed out by Edmonds et al. in a recent review on the electronic structure of GaMnAs studied by synchrotron radiation, the Mn d-states are neither fully localised or fully metallic. In addition, a clear separation between valence and impurity band is not observed experimentally. While both models offer predictive power the limitations of each have to be considered in their application.[22]

### 1.3.2 Interstitial Mn and lattice location

Even though interstitial manganese fulfils such an important role in the existence of the ferromagnetic state, either by reducing the hole and localised spin concentration as in the p-d zener model, or by determining the Fermi level location in the impurity band model, its nature is still not fully understood. Currently it is accepted that $Mn_i$ is a low temperature diffuser at about 200° C.[23] The first improvements in $T_c$ were made by

post-growth annealing at growth temperature with measurements showing that the $Mn_i$ outdiffuses towards the surface to form an oxide layer or MnAs monolayer if capped with As.[24] Currently, progress has halted with concentrations above 10% not leading to higher $T_c$.[25] Better understanding of the exact nature of the diffusion mechanism and location of the interstitial manganese is necessary to perfect growth and post-growth processes, hopefully opening up the possibility of room temperature ferromagnetism.

The lattice location of interstitial manganese has been debated since the first synthesis of (Ga,Mn)As with the first EXAFS(extended x-ray absorption fine structure) measurements showing only substitutional manganese.[26] Later EXAFS and ion channeling experiments painted a picture of a combination of gallium substitutional manganese and a smaller fraction T site interstitial manganese.[27][28] On basis of the electron structure of Mn one would expect interstitial Mn to be coordinated by arsenide atoms just as substitutional Mn. However more recent EXAFS measurements determined the T site to be $T_{Ga}$[29] that is, Mn coordinated tetrahedrally by gallium cations while anomalous x-ray diffraction experiments found both $T_{Ga}$ and $T_{As}$ in comparable fractions.[30] This implies that the presence of surrounding $Mn_{sub}$ atoms could affect which T lattice location is energetically more favourable, depending on whether $Mn_{int}$ is free, or present in Mn complexes. Lastly, transmission electron microscopy measurements indicated that $Mn_{int}$ occupies predominantly the $T_{As}$ site.[31]

With the controversy surrounding the lattice location of $Mn_{int}$ on the experimental side it is interesting that ab-initio DFT calculations demonstrated the $T_{As}$ tetrahedral position to be lowest in energy, regardless whether it is isolated $Mn_{int}$ or present in $Mn_{int}$-$Mn_{sub}$ pairs or $Mn_{sub}$-$Mn_{int}$-$Mn_{sub}$ triplets.[32] Considering the importance of interstitial manganese for the material properties of (Ga,Mn As), determining its lattice location(s) unambiguously, that is the $T_{As}$ or $T_{Ga}$ site or a mixed minority occupancy, was of paramount importance. Emission channeling (EC), discussed in detail in section 2.2.2, is ideally suited to distinguish between $T_{As}$ and $T_{Ga}$ and experiments performed by Pereira et al. on (Ga,Mn)As in the ultra-dilute regime ( $< 0.05\%$) found only minority occupation of the $T_{As}$ site[33][34], in agreement with the DFT calculations. However there was still the possibility that higher impurity concentrations and the concomitant $Mn_{sub}$ presence would lower the defect energy of the $T_{Ga}$ site. Recent results from EC performed by T. Lima et al. on (Ga,Mn)As samples at higher impurity concentrations (1-5 %) show that $Mn_{int}$ occupies the $T_{As}$ site with no other other interstitial positions being occupied and no dependence on the presence of surrounding substitutional Mn.[35] In this work the lattice location and diffusion behaviour of Mn in an ion implanted pulsed laser melted (II-PLM) sample as opposed to the MBE samples in the earlier work by L.M.C. Pereira and T.A.L. Lima is studied. Due to the different growth-method and depth profile of

electrically active $Mn_{Ga}$ the diffusion behaviour of Mn is affected. This offers extra evidence as to which mechanisms underlie the diffusion. The differences in structure and its importance for the diffusion behaviour is discussed in sections 2.1 and 3.1.3.

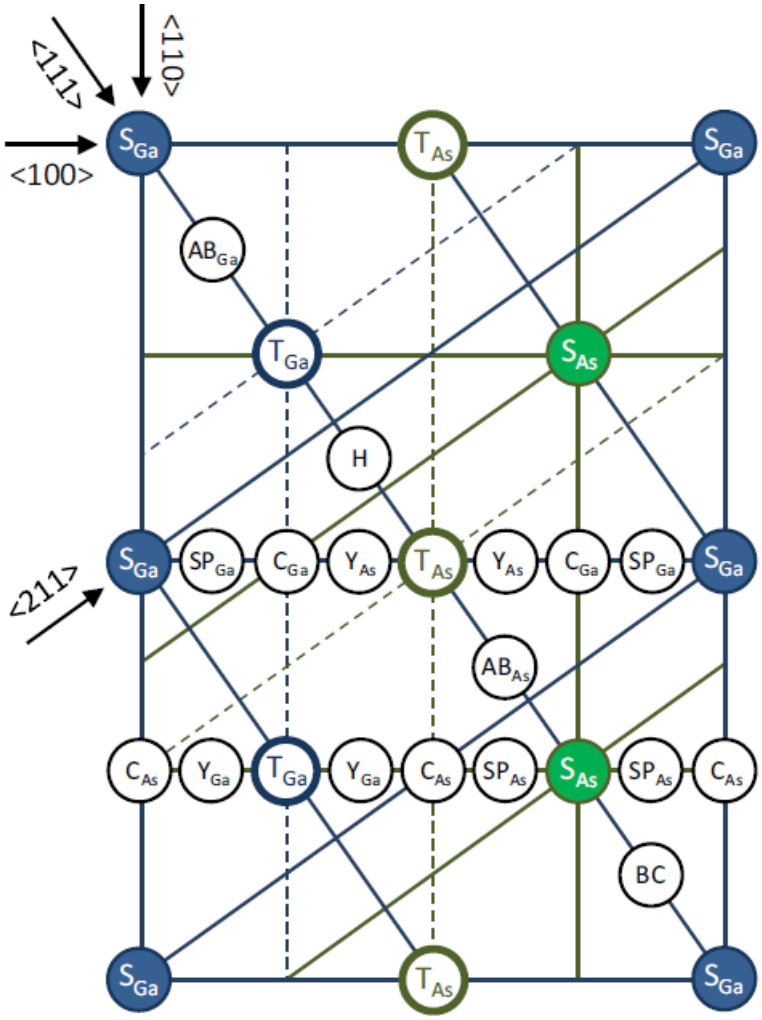


Figure 1.1: The ⟨110⟩ plane in zincblende GaAs. Possible lattice locations of Mn are the substitutional Ga and As sites ($S_{Ga}$ and $S_{As}$), the tetrahedral Ga and As sites ($T_{Ga}$ and $T_{As}$, the bond centered (BC) and anti-bonding sites ($AB_{Ga}$ and $AB_{As}$) and the C, Y and split interstitial sites ($SP_{Ga}$ and $SP_{As}$). [34]

## 1.4 GaN

### 1.4.1 Lattice and Phase diagram

GaN is a III/V wide band-gap semiconductor used in the blue LED industry and for its high-power/high-temperature characteristics in the semiconductor industry. It crystallises in the wurtzite (hexagonal) structure with the Ga cation coordinated tetrahedrally by the N anions and vice versa. It is usually grown on sapphire or SiC substrates by molecular beam epitaxy(MBE) or metal-organic chemical vapor deposition (MOCVD)). [36] It can also be grown in the meta-stable zincblende (cubic) structure by epitaxial growth on a GaAs or SiC substrate. In the context of DMS GaN is doped with a transition metal (Fe, Co, Mn) at concentrations between 1 to 10%. Higher concentrations up to 38% have also been studied but then the interest is rather in the magnetic properties of the secondary phase precipitates. In general the structure of TM-doped GaN depends on a combination of impurity concentration, growth mechanism and growth temperature. At higher temperatures/impurity concentration the sample will not be uniform in concentration but become chemically segregated, showing a variation in TM impurity concentration throughout the crystal. At further increased growth temperature and concentration precipitates will form which can have a different crystal or chemical structure compared to the bulk. This can be shown visually in the phase diagram shown in figure 1.2.

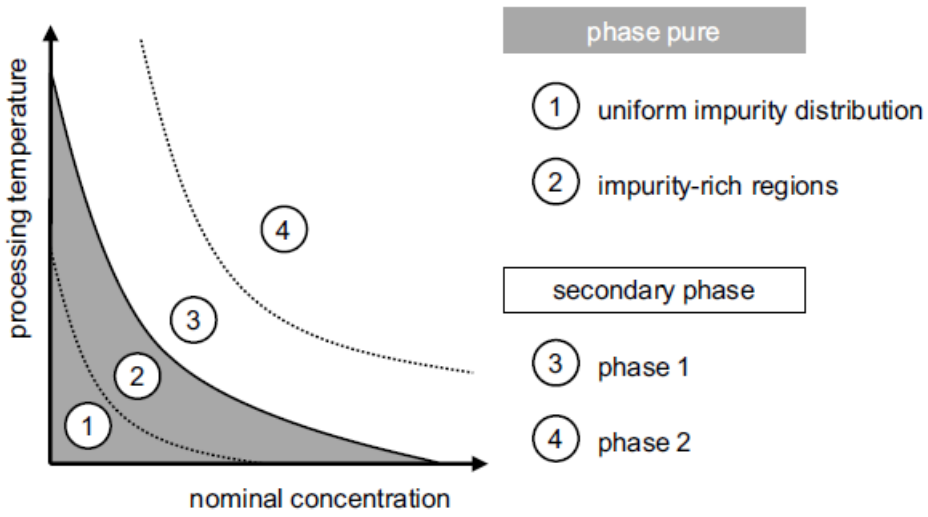


Figure 1.2: Schematic phase diagram of GaN in function of growth temperature and impurity concentration. The actual phase will depend on other factors as well such as the growth method.

### 1.4.2 Lattice location and properties of Mn in GaN

In the phase-pure region of the phase diagram Mn will be incorporated substitutionally or on interstitial lattice sites. Due to the chemical similarities and comparable ionic radius of Mn and Ga one can expect Mn to be incorporated on the Ga site. This has been confirmed by XAFS[12][37] and channeling[38] measurements. Nevertheless evidence of anion and interstitial occupancy has been found as well in zincblende GaN by XAFS[39] and wurtzite GaN by EC[40] experiments. More detail can be found in section 3.2.1. Possible lattice sites are shown in figure 1.3

Since Ga and N bond tetrahedrally by s-$p^3$ hybridisation, Mn on the Ga site will have to offer 3 electrons. The valence electron structure of Mn is $3d^5 4s^2$ and hence one possible charge state of the Mn cation is then 3+ ($3d^4$). However, when the Fermi-level is near the conduction band minimum (CBM) the required third electron can be brought from a donor site and Mn will incorporate in the 2+($3d^5$) charge state. While the cause is still controversial (native point-defects, impurities incorporated during growth)[41] GaN is naturally n-type and both $Mn^{2+}$ and $Mn^{3+}$ can coexist in the crystal.[42]

Compared to Mn in GaAs (0.1 eV above the valence band maximum (VBM)) the Mn 2+/3+ transition level is located about 1.8 eV above the VBM. Since this is a deep level, no free holes are offered by the substitutional Mn. Due to free charge carriers being a necessary ingredient in the Zener model for ferromagnetism this has to be compensated by doping the GaN crystal to achieve the required charge concentrations. The deep level of Mn in the bandgap of GaN makes the application of the Zener model even more tenuous for another reason. The spin-split bands are the result of an exchange energy due to the hybridisation between the Mn *3d* states and the *s-p* host states. If the Mn d-state level is deep it will be too far removed from the *s-p* levels for hybridisation to occur. This implies that for the mean-field Zener model to be applied in GaN substantial modifications are needed.[42]

### 1.4.3 Magnetic ordering

In wide-band gap DMS in general, and GaN specifically, in recent years several types of magnetic ordering have been observed experimentally from paramagnetism, to anti-ferromagnetism or at most ferromagnetism with very low $T_c$.[12][13][14] This stands in stark contrast with the original prediction of room-temperature ferromagnetism by Dietl. and earlier experimental results which found ferromagnetism with curie temperatures from 20 K to as high as 920 K. Historically, 5 % TM doped GaN with a hole concentration of $3.5 \times 10^{20}\mathrm{cm}^{-3}$ was predicted to be ferromagnetic at room-temperature by Dietl et al. in

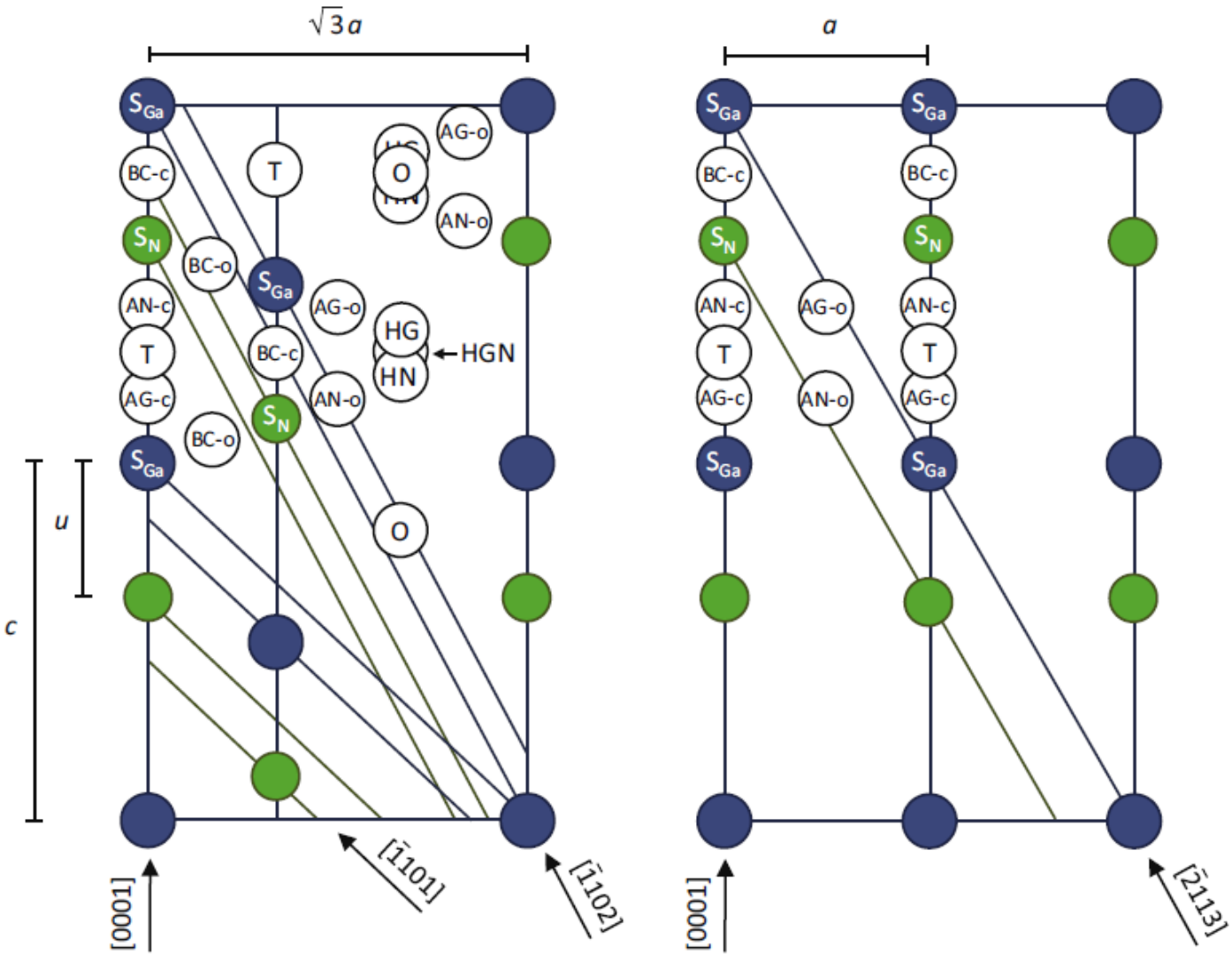


Figure 1.3: The $(11\bar{2}0)$(a) and $(11\bar{1}0)$(b) planes in wurtzite GaN showing the possible lattice locations for an implanted TM. These sites are the substitutional $S_{Ga}$ and $S_N$ sites as well as the following interstitial sites: bond centered (BC), anti-bonding gallium and nitrogen (AG and AN), tetrahedral (T), hexagonal gallium and nitrogen (HG and HN) and octahedral (O). Since it is a wurtzite structure two non-equivalent directions with corresponding non-equivalent sites are present. The suffix -c or -o denote sites respectively on the crystal axis and along the basal direction.

2000 through a mean-field Zener model.[11] Not long after, many experiments confirmed the presence of ferromagnetism in GaN and other wide band-gap DMS which was at first received with scepticism since even nowadays the highest hole concentration achieved in p-type GaN are of the order of $10^{18}\text{cm}^{-3}$ . Hence at first any observed magnetism was attributed to the presence of precipitates or measurement artefacts. However with evidence of ferromagnetic ordering in wide band-gap DMS piling up, other models for room-temperature ferromagnetism in these materials started to be developed from the theoretical side. In the rest of the section some of these models will be introduced, and

mechanisms counteracting ferromagnetism explained.

**Short-range interactions:** Since according to the mean-field zener model not enough free charge carriers are present for long-range ordering it makes sense to consider possible sort-range interactions. In general these are the direct exchange interaction, indirect superexchange and the double exchange. The direct exchange interaction, where the magnetic interaction is a result of a direct overlap of the magnetic orbitals can be dismissed out of hand since the Mn cations in GaN at the relevant concentrations ( $x \approx 10\%$) are too far apart to interact directly. Indirect superexchange where the magnetic cations interact through an intermediate non-magnetic ion ($N^{3-}$) is another possibility, however this is exchange is usually anti-ferromagnetic. Lastly, the double exchange which requires the presence of two different charge states of the magnetic cation is indeed ferromagnetic but while it may play a role in some of the wide band-gap DMS where ferromagnetism is observed the requirement of different charge states is for most of them not fulfilled. While both superexchange and double exchange can be present and influence the ordering they are unlikely to result in the ferromagnetism observed at room-temperature. Since these interactions are short-range they can only lead to total ordering when all Mn is linked in nearest-neighbour paths i.e. in the form of a percolation cluster. As the percolation threshold is at an impurity concentration of $x \approx 20\%$ for wurtzite GaN and the observations of ferromagnetism were at concentrations half of this, this rules out any short-range interaction as the dominant mechanism.

**Long-range interactions**: Since the mean-field Zener model required much larger hole concentrations than ever realised in GaN other, more exotic, models were proposed which could offer long-range order without the stringent charge carrier requirement. All these models have one feature in common: the presence of defects other than the TM substitution in the form of vacancies, self-interstitials or surface defects. An example of this is the bound magnetic polaron (BMP) model [43]. In the BMP model electrons related to shallow defect donors form an impurity band. These electrons can couple to the magnetic moment of the TM cation forming a magnetic polaron quasiparticle. At a critical donor concentration metallicity sets in and the electrons become delocalised thus creating a large radius for the magnetic polarons. While the concentration of Mn atoms is still below their percolation threshold, the percolation threshold of the magnetic polarons is much lower due to their larger radius. In this way the cations could be lined up ferromagnetically at the observed low concentrations.

In light of more recent, carefully controlled, experiments which found only the absence of room-temperature ferromagnetism in (Ga,Mn)N, it seems we have to defer to the original, carrier-mediated mechanism to achieve ferromagnetism. Due to the low possible hole concentration in p-type GaN this seems unlikely. However anti-ferromagnetism and low-

temperature ferromagnetism has been found. Clarification for these contradictory results, came by Bonanni et al. in 2011.[44] The magnetic interaction of $Mn_{Ga}$ ions was shown to depend on its charge state (see 1.5.2) , from ferromagnetic in the 3+ charge state to anti-ferromagnetic in the 2+ charge state. When stringent growth conditions are not observed compensating defects such as the N vacancy and H impurities are present which will cause $Mn_{Ga}$ to be in the 2+ charge state and hence, couple anti-ferromagnetically. As there is evidence that Mn ions could also incorporate interstitially or even on the anion site, these potential donor defects may also electrically compensate the ferromagnetically interacting $Mn_{Ga}{}^{3+}$ to anti-ferromagnetically interacting $Mn_{Ga}{}^{2+}$. Therefore, determining the lattice location of Mn in GaN and (Ga,Mn)N is of interest for a deeper understanding of their magnetic properties, which even if room-temperature ferromagnetism is not realised in these specific materials, may guide and aid the development of new DMS materials.

## 1.5 Crystal defects

While it is usually not discussed in this manner, the study of DMS is essentially, the study of defects in the form of substitutional and interstitial TM dopants in the semiconductor crystal. But even if these wanted impurities are not considered, many other crystal defects can be formed during growth and in the case of emission channeling, implantation. Not only will this affect the structural and magnetic properties of the DMS by potentially trapping the TM dopants in defect complexes but, since defects can also be charged, the Fermi-level as well. In this section first different types of defects will be introduced and the concept of charge states explained.

### 1.5.1 Defects and defect complexes

A perfect crystal, consisting of a near-infinite repetition of the crystal cell is only an idealisation; all crystals will contain defects. At finite temperature the creation of a defect increases the entropy, which is accompanied by a decrease in the Gibbs free energy, the relevant parameter when discussing defect formation. In general the concentration of a given defect is given by:

$$c_{defect} = N \exp\left(\frac{-G_F}{k_b T}\right) = N \exp\left(\frac{-E_f}{k_b T}\right) \exp\left(\frac{S}{k_b}\right).$$

Here N is the number of sites where the defect can be incorporated, $G_F$ and $E_f$ are the free and formation energy respectively and S is the entropy which is the sum of a configurational and vibrational part. This leaves us with the calculation of the formation

energy which isn't constant but depends on the growth conditions of the crystal. More specifically, it depends on the chemical potentials $\mu_{Ga}$ and $\mu_N$ which describe the reservoir from which the gallium and nitrogen atoms are taken or brought in order to create the defect. If the defect is charged (which will be described in more detail further on) the formation energy also depends on the position of the Fermi level($E_f$) from which electrons are taken to charge the defect. Putting all this together:

$$E_f(q) = E^{tot}(q) - n_{Ga}\mu_{Ga} - n_N\mu_N - qE_f. \tag{1.1}$$

Here q is the charge state of the defect, $n_{Ga}$ and $nN$ are the total number of Ga and N atoms and $E^{tot}(q)$ is the total energy of the crystal with the defect. Of course now the difficulty of calculating the formation energy is shifted to the calculation of the total energy of the system. Theoretical tight-binding or DFT calculations keep this calculation tractable by only considering a supercell, containing several unit cells. Care has to be taken to include finite-size and other effects and perform a good sampling of points in k-space which is why formation energies determined in this way are only semi-quantitative. Since in emission channeling ions are implanted within the crystal at high energies one needs to distinguish between native defects which involve only Ga and N, and impurity related defects which also incorporate the implanted ion. Native point defects can be interstitials, vacancies or antisites. A vacancy is the lack of an atom on its typical lattice site and can be considered a particle in its own right, it can diffuse and interact with other atoms and vacancies. This is a consequence of the movement of the surrounding atoms and in this respect it is very analogous to the hole/electron duality where the movement of electrons is reinterpreted as the movement of a hole with opposite momentum. Interstitial atoms are atoms displaced from their ideal lattice sites. In compound crystals, antisites can be formed which is the presence of an atom of type A on the lattice site of a different atom of type B in the compound. Defects of higher dimensionality such as dislocations (line-defect) and grain boundaries(planar defect) also exist but do not concern us in this work. One special case of a point defect is the Frenkel pair, a vacancy-interstitial pair generated by the movement of a substitutional atom towards an interstitial site leaving behind a vacancy. Note that despite the attractive coulomb interaction there is no requirement for this pair to stay close together, at high temperatures both can diffuse throughout the sample.

When an impurity is implanted in the sample it can take up as many non-equivalent substitutional sites in the crystal as there are chemical types of atoms in the compound. Just as for native defects also interstitial sites can be occupied, usually sites of high symmetry within the lattice. With each of these lattice sites a certain formation energy is associ-

ated. When the impurity is incorporated during growth in thermodynamic equilibrium it will occupy the site(s) lowest in formation energy. In out-of-equilibrium processes such as MBE growth or ion implantation this is not necessarily the case and also defects with high formation energies can exist in large amounts.
Defect complexes are the result of minimization of total energy when two or more defects are brought together in each others neighbourhood. Common complexes are A-B complexes, consisting of two defects. Of these, impurity-defect complexes are most important to this work and are the coupling of an impurity, either in a substitutional or interstitial site and a non-impurity defect in the form of a vacancy or an interstitial. Also possible is the so called split-vacancy interstitial in which two vacancies on substitutional positions coordinate an interstitial impurity.

### 1.5.2 Defect charge states

When electrically doping a host semiconductor with an impurity to induce extra charge the naive view is that the added electron or hole is immediately available. A more careful analysis can be made by adapting the Bohr model of the hydrogen atom. Assuming that the added charge carrier is an electron it will move in a screened coulomb potential of the positive impurity atom. Taking into account the dielectric constant of the medium and the effective mass of the electron energy levels can be calculated analogous to the energy levels of the electron in the hydrogen atom:

$$E_n = E_\infty - m_e^* \frac{13.6eV}{\epsilon^2 m_e}$$

with $m_e^*$ the effective mass and $\epsilon$ the dielectric constant of the host semiconductor. $E_\infty$ is the energy at which the electron is ionised, or the conduction band edge in the band diagram. Using the equation above, a binding energy of 10-100 meV is found in semiconductors. At room temperature the electrons can have enough thermal energy to ionise and become conduction electrons. The same model also applies to holes, however now the energy levels will be above the valence band edge since it takes energy to take an electron from the valence band and put it in the defect state. From now on these states will be referred to as respectively *donor* and *acceptor* states and the impurity ions as *donors* and *acceptors*.

However these shallow, hydrogenic levels are not the only possible states an impurity can induce. So called deep levels are also possible, which as the name suggests, tend to be located deep in the band-gap. To understand the origin of these states one has to consider

the full Hamiltonian:

$$\hat{H} = \hat{H}_0 + V_{imp}$$

Where the impurity potential $V_{imp}$ is given by:

$$V_{imp} = V_{lr} + V_{sr}$$

with $V_{lr}$ the long-ranged, screened coulomb potential and $V_{sr}$ the short-ranged central cell potential due to the chemical differences between the impurity atom and the host semiconductor and lattice distortions. In the derivation of the energy levels of a hydrogenic, shallow defect, we have implicitly ignored the short-ranged potential. This is allowed because in fact shallow electron states have little charge left in the region around the impurity. Because they are delocalised states in real space the effect of the host semiconductor can be absorbed in the dielectric constant. However if the electron states are localised in real space the interaction with the valence electrons become important and the hydrogenic, one particle model breaks down. In the modern framework the original meaning of deep levels, i.e. deep in the band-gap, has been abandoned. The current interpretation is that shallow levels are energy states resulting from the long-range screened coulomb potential and deep levels are produced by the short-range part of the impurity potential. It is thus also possible for localised, deep levels to be present close to the CBM or VBM.

We are now in a position to understand transition levels and charge states of impurities. As mentioned before, most impurity defects cannot be described as simple hydrogenic defects and the full many body system of the impurity and valence electrons needs to be considered. The position of a transition level with respect to the conduction band is then defined as the energy required to remove an electron from the impurity and place it in the conduction band. In this way the transition level is characteristic of two defect states, the impurity with n electrons before, and n-1 electrons after removing it. Defining the neutrally charged defect to have $n_0$ electrons a ladder of transition levels can be defined with defect states containing more electrons above in the band diagram and defect states with less electrons below. An impurity in a transition level above the CBM will ionise and lose it's electron to the conduction band where it will scatter to the lowest level. Conversely, if the impurity is in a transition level below the VBM it will be filled.

Which transition level(s) will be stable depends on the position of the Fermi level. Assume we have a neutral defect with a transition level in the bandgap. If the Fermi level is lowered towards the VBM it will eventually become less and less likely for the neutral charge state to be stable and an electron will drop down to the Fermi level, leaving the impurity in a state with $n_0 - 1$ electrons. On the other hand, if the Fermi level is increased towards the

CBM at a certain point an electron will be taken from the Fermi level and the impurity will have $n_0 + 1$ electrons. This effect is taken into account explicitly in equation 1.5.1.

Usually rather than use the amount of electrons to define the transition level the charge state q of the defect is quoted since it more directly informs the level of ionisation of the defect. There are different conventions in defining the charge state of an impurity. In the case of an ionic solid with large differences in electro-negativity it is natural to treat the constituent to good approximation as fully ionised. However in covalent crystals this description in terms of ions becomes rather artificial and a different approach is used. The charge state of an impurity is then defined as the extra charge induced locally. For example, a Cr atom will substitute in the ionic crystal MgO for the Mg atoms in the 3+ charge state corresponding to the electron structure $3d^3$. When the same Cr atoms substitute for Ga in GaP three of its electrons will participate in the bonding leaving the electron structure $3d^3$. the charge state is then defined operationally to be $Cr^{3+}$.

In the rest of this work the this operational convention will be used and $\epsilon(q/q')$ is the transition level of defect from charge state q to charge state q'. As the amount of electrons that participate in the binding will define the neutral state, the transition levels of intersitial and substitutional Mn will be different. For example, in a trivalent semiconductor such as GaAs and GaN, the $\epsilon(3+/4+)$ charge state will be the fourth donor level of interstitial Mn whereas it is only the first donor level for substitutional Mn. This is because three electrons participate in the binding and hence $Mn^{3+}$ is the neutral charge state.

# Chapter 2

# Experimental and growth techniques

## 2.1 Growth techniques

### 2.1.1 Molecular beam epitaxy(MBE)

Any technologically interesting application of GaMnAs will require high concentrations of Mn impossible to achieve in equilibrium conditions due to the solubility limit of transition metals in the III-V host semiconductor. LT-MBE which overcomes the solubility limit by non-equilibrium growth conditions, was first used to grow InMnAs where the effect of the substrate temperature ($T_s$) in epitaxial growth was first observed.[8] At substrate temperatures higher than 400° C the grown InMnAs film was porous and did not adhere to the surface. Only when $T_s$ was in the range of $200° - 300°$ C was epitaxial growth observed. Epitaxial growth of GaMnAs with LT-MBE was first performed in 1996 by the group of H. Ohno.[9] First a GaAs substrate layer is formed by regular MBE, usually at temperatures of around 600° C. Next, $T_s$ is lowered to about 200° C while the As effusion is kept constant. The shutters in front of Ga and Mn Knudsen effusion cells are consecutively opened leading to to the epitaxial growth of $Ga_{1-x}Mn_xAs$ as monitored during deposition by RHEED (reflection high energy electron spectroscopy). [45] The depth profile of manganese achieved after this growth method is more or less constant over the thin film due to the epitaxial growth.

### 2.1.2 Ion implanted- pulsed laser melting (II-PLM)

A second, more recent, technique to grow GaMnAs thin films, is ion implanted pulsed laser melting (II-PLM) pioneered by Scarpulla et al. in 2003.[46] Ion implantation is a classic technique in the semiconductor industry based on a simple principle. Atoms or molecules are created at an ion source, electrostatically accelerated to high energies, sent through a mass separator and steered into an implantation chamber where the ions impinge on the sample. Ion implantation will create a variety of lattice defects such as vacancies, interstitials and dislocations. After implantation the GaMnAs thin film will have a gaussian manganese depth profile but thermal annealing is still necessary both for damage recovery and dopant activation. Rapid thermal annealing (RTA) of a few seconds, above growth temperature ($\approx 900^\circ$ C), will lead to the formation of precipitates and secondary phases. Even flash-lamp annealing (FLA) on the order of a few ms results in low Curie temperatures and small magnetic moments. Only pulsed-laser melting (PLA) on a time-scale of micro-seconds has been shown to result in Curie temperatures comparable to LT-MBE.[47] During PLA the GaMnAs surface reaches temperatures up to $1500^\circ$ C causing the crystal to melt ( $T_{melt} \approx 1240^\circ$) and recrystallise. The solubility limit of dopants is much higher in the melt phase and during the epitaxial reformation the magnetic dopants are incorporated over their room-temperature solubility limit in the solid phase. The fast cooling rate of PLA ($10^{11} K/s$) is responsible for the lack of secondary phase growth. After this procedure the formerly gaussian depth profile formed by ion implantation will be more homogeneous than before but still show a much larger gradient in concentration than an MBE sample. A typical depth profile, acquired by secondary ion mass spectroscopy of an II-PLM GaMnAs film is shown in figure 2.1. Due to the high-temperature processing the thin film is free of interstitial Mn and typical post-growth annealing is not necessary to achieve high $T_c$ [48]

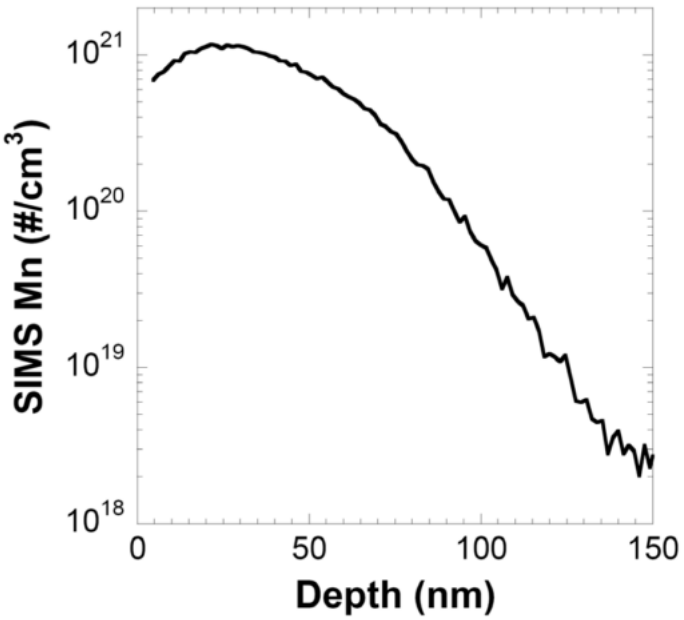


Figure 2.1: Depth profile of an II-PLM GaMnAs thin film acquired by SIMS. The Mn distribution extends to about 120 nm, has a peak concentration of 0.051 at 25 nm and a full width at half maximum (FWHM) of 60 nm. The large gradient in depth distribution is one of the key differences with MBE samples. Image taken from [48]

## 2.2 Electron emission channeling

### 2.2.1 Channeling

In order to study the lattice location of transition metals in DMS the technique of emission channeling is used. Before going into detail first the general principle of channeling will be explained. The basic idea is very simple, an energetic positively charged particle going through the crystal lattice will interact with the surrounding ions and depending on the crystal direction it will 'see' a different structure through which to penetrate. Mostly, the interaction is given by the screened coulomb interaction and if the motion of the particle is along a crystal axis or crystal planes it will be steered by several small-angle collisions and penetrate further compared to the 'random' direction. These directions are illustrated in figure 2.2.

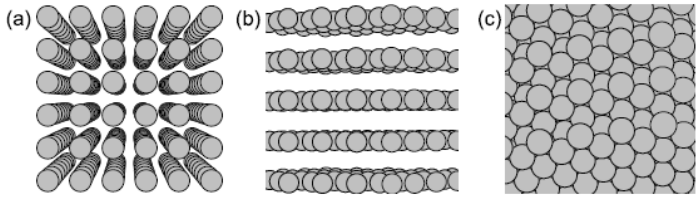


Figure 2.2: Projection of a cubic lattice as seen from three different directions. The directions along which the projection is ordered will lead to (a) axial channeling, (b) planar channeling and the unordered projection is along a random direction. [49]

### 2.2.2 Emission channeling

One specific application of channeling is the technique of emission channeling (EC). First, radioactive probe atoms are implanted in the sample to be studied. An implanted radioactive probe atom will, after decay, emit either electrons, alpha particles or positrons depending on the decay mechanism. These charged particles, isotropically emitted, will experience a screened coulomb interaction with the surrounding atoms resulting in channeling. The particles leaving the crystal will be measured with a 2D position sensitive detector as a characteristic emission pattern, revealing the particular position of the introduced impurity.

Emission channeling has a few clear advantages compared to more conventional techniques such as Rutherford backscattering (RBS), particle induced x-ray emission (PIXE) and nuclear reaction analysis (NRA). Firstly, the comparison between experimental 2D patterns and simulated patterns offers unambiguous and quantitative lattice location determina-

tion superior to the more indirect determination of other ion channeling techniques. The most widely used of these, RBS, relies on elastic recoil of the ions which makes discriminating between lighter impurity atoms in the host lattice consisting of heavier atoms very difficult. This is the case for both (Ga,Mn)As and GaMnN, which is one of the reasons RBS is ill suited to study the lattice location of Mn in these DMS materials. Another advantage of EC is its sensitivity, down to $10^{-12}$ atoms $cm^{-2}$ compared to a fluence of $10^{14} - 10^{15}$ atoms $cm^{-2}$ for RBS. This implantation fluency is directly related to the damage levels in the sample since an incoming ion will lose energy by nuclear and electronic loss mechanisms. This will cause a displacement of atoms and even collision cascades at high enough energy. At high enough doses amorphisation is observed and the crystal structure is lost. Since GaAs is an example of a material with a low amorphisation threshold ( $4 \cdot 10^{13}$ atoms $cm^{-2}$) [50] it is especially important to use low implantation doses which increases measurement time with RBS enormously. A third advantage is that emission channeling can be applied to cases where the impurity atom occupies several lattice sites in different fractions. Something which, while possible, is quite difficult with other, more conventional techniques.

In all but one experiment in this thesis implanted $^{56}$Mn was used. It will decay by $\beta^-$ decay and its reaction is given by:

$$^{56}\mathrm{Mn} \rightarrow {}^{56}\mathrm{Fe} + e^- + \bar{\nu}$$

The outgoing electron will have an energy varying between zero and the maximum energy provided by the decay since it is a three body process. Since the emitted electron is attracted to the positive ions in the lattice it will channel along the rows and planes rather than between them. One condition for channeling to happen is for the momentum of the particle to be along the potential minima. As the electrons are emitted isotropically a fraction of them will experience a wide-angle deflection and be scattered rather than channeled. These so-called channeling and blocking effects, depending on the position of the radioactive probe atom, are illustrated in figure 2.3. Due to the low mass of the electron, its motion can not quantitatively be described with the classical picture of coulomb interaction between the electron and the crystal ions and the system has to be solved quantum-mechanically. This will be explained more fully in section 2.2.4.

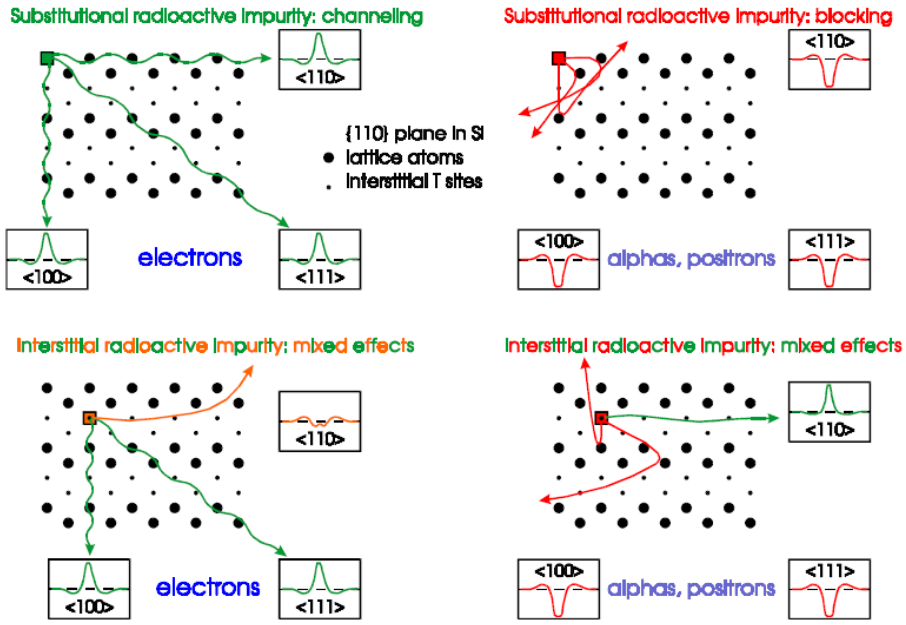


Figure 2.3: Principles of channeling and blocking effects, shown for positive and negative particles on substitutional or interstitial positions.

### 2.2.3 Experimental set-up

#### Ion implantation

The starting point of the ion implantation at ISOLDE is the proton beam delivered by the proton synchrotron booster facility (PSB). This proton beam with an energy of 1.4 GeV and a current of up to 2 mA will radiate upon a thick target which in our case is $UC_2$. The high-energy protons will induce either fission, spallation or fragmentation of the uranium nuclei leading respectively to medium-weight, heavy and light radionuclides ( cfr. figure 2.4 ). In the context of emission channeling the neutron-rich nuclides generated by fission are the most interesting since they will decay by the $\beta^-$ process. The next step is to ionise the nuclides to be able to select, and steer them towards the target. This is done by using a resonant laser ion source which will stepwise excite the nuclides through two or three atomic transitions.[51] To achieve this, the laser energies are finely tuned to the energies of the atomic transitions. Since these atomic transitions are element specific the ionisation is chemically selective which improves the beam purity. After this the ionised nuclides are extracted and accelerated by an extraction electrode with an energy chosen between 30-60 keV. The next step is to separate the nuclides which can be done either in the general purpose separator (GPS) or high resolution separator (HRS). Both use a magnetic field to separate the by mass and finally the nuclides are steered by electrostatic quadrupole elements towards the beam line where after collimation and another round of focussing they will reach the sample.

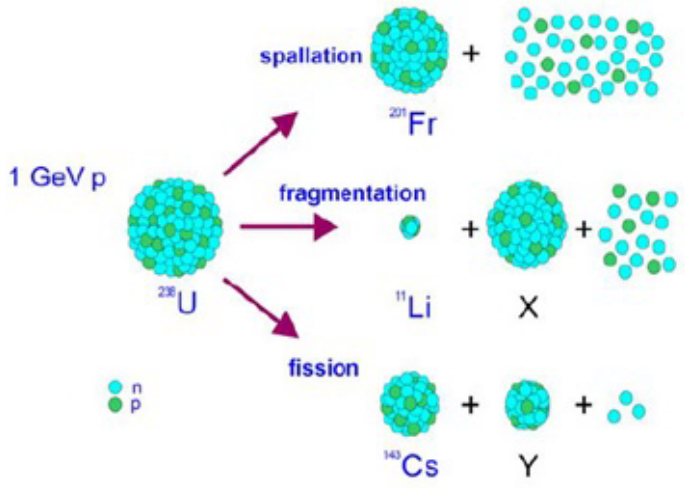


Figure 2.4: Possible nuclear reactions after a high-energy proton hits an uranium atom leading to fission, fragmentation or spallation. Taken from [52]

**Set-Up**

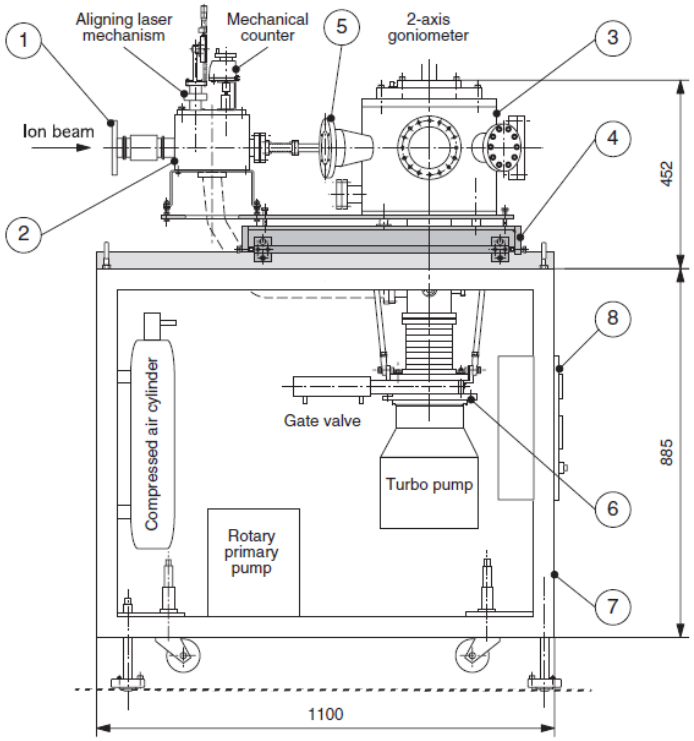


Figure 2.5: Schematic view of the EC chamber assembly with dimensions in mm: (1)ISOLDE beam-line flange, (2)collimation block, (3) experimental chamber, (4) XZY sliding orientation cradle, (5)detector flanges, (6) vacuum block, (7) movable supporting frame stand with wheels and adjustable supporting pads, (8) auxiliary control equipment panel. [53]

For a long time, emission channeling using electron emitting radio-isotopes was limited to long-lived isotopes with half-lives above 6 hours due to the count rate level of the detection systems available. This changed with the recent development of fast, self-triggered Si pad detectors reaching count rates of up to 4000 events per s.[54] This development made the use of short-lived isotopes feasible leading to the division of emission channeling experiments in so called off-line experiments, in which the implantation of the samples and the measurement of the emission pattern are done separately, and on-line experiments in which both are done in the same chamber even allowing one to implant and measure concurrently. The three most important parts of the set-up (shown in figure 2.5) are the vacuum chamber, the 2-axis goniometer and the detection pad. The vacuum chamber ($\leq 10^{-5}$mbar) is created and maintained by a rotary vane pump and a turbo molecular pump for respectively the rough and fine vacuum. The sample is oriented by the 2-axis goniometer towards the position-sensitive detection pad which is $32 \times 32$cm$^2$ large consisting of 22 by 22 channels. Annealing is performed by the electrical heating of a tungsten wire attached to the sample holder. A cooling system is in place to keep the

detector temperature at room temperature, necessary to minimise noise levels.

#### Data measurement

The experimental angular resolution of the emission pattern is determined by the distance between sample and detector, the beam spot size and shape and lastly the detector position resolution which depends on the energy and nature of the incoming particle. Notice that the goniometer precision does not affect the angular resolution since the detector is two-dimensional. Assuming that both the projected beam spot (the area from which particles are emitted) and the detector position resolution can be described by isotropic two-dimensional gaussian distributions one finds from geometrical considerations that the angular resolution is given by:

$$\Delta\theta = \arctan \frac{\sqrt{\sigma_{spot}^2 + \sigma_{det}^2}}{D} \approx \frac{\sqrt{\sigma_{spot}^2 + \sigma_{det}^2}}{D}. \tag{2.1}$$

Here D is the distance between sample and detector. A natural limit on the detector resolution is given by the lateral straggling of the detected particles. The maximum electron range for electrons in silicon varies from 7$\mu$m at 30 keV to 2mm at 1 MeV. At the electron energies in our EC experiments the lower limit is given by the pad size of 1.45 mm. The beam spot resolution is limited by the difficulty to achieve a beam focussed to less than 1 mm diameter for implantation. Usually a distance of 30 cm is used for an angular range of about 6° and an angular resolution of 0.1°. If even higher resolution is needed the sample-detector distance is raised but at the cost of angular range.

### 2.2.4 Data Analysis

#### Manybeam simulations

The measured emission patterns are to be compared with theoretical simulations done with the manybeam software. The software was developed in the early 90's by Lindhard and Hofsäss[55] and modified by Wahl.[56] Fast charged particles emitted during the decay travelling along a planar or axial channel are described by separating the longitudinal motion and the transverse motion. The individual atomic potentials are approximated by a transverse continuum potential by averaging over the rows or planes. The full calculation of the electron wavefunction has to be done relativistically by solving the Klein-Gordon equation. Since the continuum potential does not depend on the longitudinal coordinate the resulting wave function can be split in a longitudinal relativistic, time dependent part

and a stationary transverse part. The transverse motion of the electron is much lower in energy and is a solution of a "transverse schrödinger" equation. By virtue of the crystal periodicity the continuum potential and electron wave functions can be expanded in a Fourier series with the same periodicity. Taking only a finite amount of Fourier components (corresponding to the "beams" in the eponymous manybeam method) solving the transverse schrödinger equation reduces to an eigenvalue problem which is easily done numerically by current computers. The potentials used are the so-called Doyle-Turner potentials which are based on Hartree-Fock calculations and consist of a sum of parametrised gaussians.
The manybeam software uses as input the lattice structure as determined crystallographically and the rms thermal vibration amplitude of the crystal atoms. For a given channeling axis, probe atom and lattice location of the probe atom a 2D emission pattern is generated. This pattern is smoothed by a gaussian with $\sigma = 0.1^\circ$ to account for the beam spot width. The detector resolution is taken into account by averaging the emission pattern over each detector cell or pixel. Each pixel corresponds to $1.45 \times 1.45$ mm or $0.24^\circ \times 0.24^\circ$. The end result is a theoretical emission pattern $\chi(\theta, \phi)$ which can be used to fit a measured emission pattern, usually to several theoretical patterns corresponding to different occupied sites.

**Fitting procedure**

In the FDD program, developed by Wahl, the theoretical emission patterns are fitted to experimental ones as follows:

$$\chi_{ex}(\theta, \phi) = S\Big[\sum_{i}^{N} f_i \chi_{theo,i} + f_{rand}\Big]. \tag{2.2}$$

Usually at most 3 different lattice positions are fitted to avoid overfitting the experimental pattern. This is a non-linear least-squares fit with 7 degrees of freedom: S,$x_0$,$y_0$,$\phi_0$,$f_1$,$f_2$,$f_3$. Of these parameters $f_i$ is the fraction of impurity atoms located on site i, $x_0$ and $y_0$ are parameters corresponding to the 'center' of the image i.e. the coordinates corresponding to the channeling axis and $\phi_0$ is the azimuthal rotation angle by which the pattern is tilted. To ensure the best fit, a scaling factor S is left free to vary as well. Last but not least is $f_{rand}$ given by

$$f_{rand} = 1 - \sum_{i}^{N} f_i$$

the fraction of atoms which does not contribute to the anisotropy of the pattern or in other words, do not give any structural information. Physically they can be considered atoms that are present in heavily damaged or even amorphous surroundings.

### Electron background

The radioactive probe in the sample will after decay, emit $\beta^-$ electrons isotropically of which only a fraction will have their momentum in the direction of the detector. These *direct* electrons can be estimated as the fraction emitted in the solid angle $\Omega$ of the detector to the full solid angle of $4\pi$. In experiments however, larger electron counts than predicted by this ratio are always observed. This is because not all electron that reach the detector have gone in a straight path towards it. These *indirect* electrons are the result of scattering events either within the sample or from parts of the set-up. Obviously these indirect electrons offer no structural information after the scattering event and only contribute to an isotropic background. If the electrons were to have well defined energy peaks (as is the case for conversion electron decay) correcting for them would be relatively straightforward as each scattered electron will not have the expected energy and will show up in a tail behind the energy peak on the spectrum. By integrating over this tail the total count of scattered electrons is then found and can be subtracted. In the case of $\beta^-$ decay electrons with a continuous energy spectrum, this cannot be done and the correction is more involved. For this purpose the pad program was developed by De Vries [52] based on the open access Geant4 toolkit. The toolkit contains interfaces to define the geometry of the system and can simulate the interaction of particles with matter. The pad program uses a Monte Carlo algorithm to create the path of several $\beta^-$ decay electrons as they travel through the sample and the set-up, correcting for energy and momentum loss along each discrete piece of the path. On basis of these simulations an estimate is made of the fraction of indirect electrons which is used in the background correction factor:

$$f = \frac{\text{total electrons}}{\text{total electrons} - \text{scattered electrons}} = \frac{\text{total electrons}}{\text{direct electrons}}$$

This background factor can be used to rescale the patterns before the fit, or equivalently, rescale the resulting fractions.

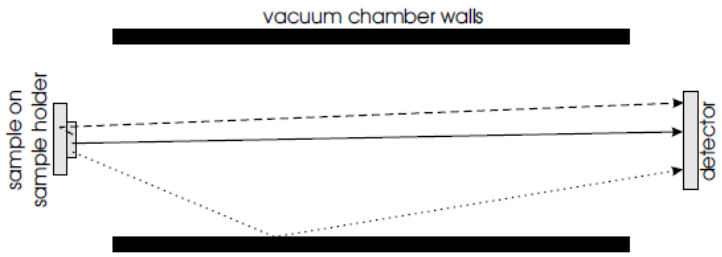


Figure 2.6: Possible paths an electron can take towards the detector. The solid line represents a direct electron while the dashed lines represent indirect electrons scattered either from the vacuum chamber wall or sample holder. Taken from [52]

# Chapter 3

# Results and discussion

## 3.1 GaMnAs

### 3.1.1 Experimental details

An II-PLM GaMnAs sample of 4-5 % impurity concentration was implanted with radioactive $^{56}$Mn ($T_{1/2}$ = 2.56 hours) probe atoms at an angle of 17° to the (001) surface to minimize ion channeling. An implantation energy of 50 keV was used, resulting in a depth profile centered around a projected range of 282 Å with a straggle of 251 Å . After implantation, measurements were made with the sample at room-temperature, annealed to 150 °C, and annealed in steps of 50 °C from 250 °C to 450°C. The measurements were made along the ⟨001⟩ , ⟨110⟩, ⟨111⟩ and ⟨211⟩ directions.

### 3.1.2 Results and discussion

#### Lattice location

Earlier emission channeling results on ultra-dilute $^{56}$Mn implanted GaAs films found only substitutional Mn and $T_{As}$ interstitial Mn (i.e. tetrahedrally oriented by As atoms)[33][34], which was also supported by ab-initio calculations.[57] Later experiments on 5% and 6% MBE GaMnAs also only saw $S_{Ga}$ and $T_{As}$ site occupation, something which is not a priori clear since interstitial manganese is also present in doublets and triplets at higher concentration.[35] This could conceivably have lowered the defect formation energy of $Mn_{int}$ on the $T_{Ga}$ location compared to the $T_{As}$ location since the former has a smaller distance between the donor $Mn_{int}$ atoms and the acceptor $Mn_{sub}$ atoms (2.45 Å versus 2.85 Å). As

there is an attractive coulomb attraction between them this lower distance would increase the binding energy of the defect and hence lower the formation energy.

In order to determine the lattice location of Mn in the II-PLM sample the emission yields were analysed as described in section 2.2.4. First a one-site fit model was used, taking into account one high-symmetry site or displaced sites between them. The sites under consideration can be found in figure 1.1 on page 7. It's important to note that the different crystal directions measured are not sensitive to all sites. For example, measuring along the $\langle 111 \rangle$ direction, both substitutional and tetrahedral sites result in the same pattern. Since it is only possible to distinguish all high-symmetry sites along the $\langle 110 \rangle$ and $\langle 211 \rangle$ directions information gathered from the $\langle 111 \rangle$ and $\langle 001 \rangle$ are best seen as offering only supplementary information. Taking this into account, by far the best fit was found for the $S_{Ga}$ site as one would expect from the valence electron structure of Mn and Ga and which is evident from the large electron count in the center of the experimental images, characteristic of substitutional sites.

Secondly a two-site fit was attempted which included $S_{Ga}$ and other high symmetry sites. The best fit was found for the $T_{As}$ site with only negligible ( $< 5\%$) fractions on other lattice locations. In figure 3.1 the experimental and theoretical emission patterns are compared. Notice how the channeling does not only take place along the rows, as indicated by the large central electron count but also along the crystal planes, evidenced by the extended higher electron counts emanating symmetrically from the center.

As mentioned in section 2.2.4, the analysis of the emission yield patterns is a mathematical least-squares fit. The goodness of the fit, quantified by the $\chi^2$ error determines which theoretical pattern(s) and corresponding lattice location(s) are considered in the analysis. However, to get a more intuitive understanding of the result, the emission pattern for the as-implanted sample was shown with the pure substitutional fit subtracted. Logically, the remainder should be the result of the Mn emitting from all other possible lattice sites. These patterns are then compared with the simulated $T_{As}$ and $T_{Ga}$ patterns illustrating the agreement with $T_{As}$ occupation visually.

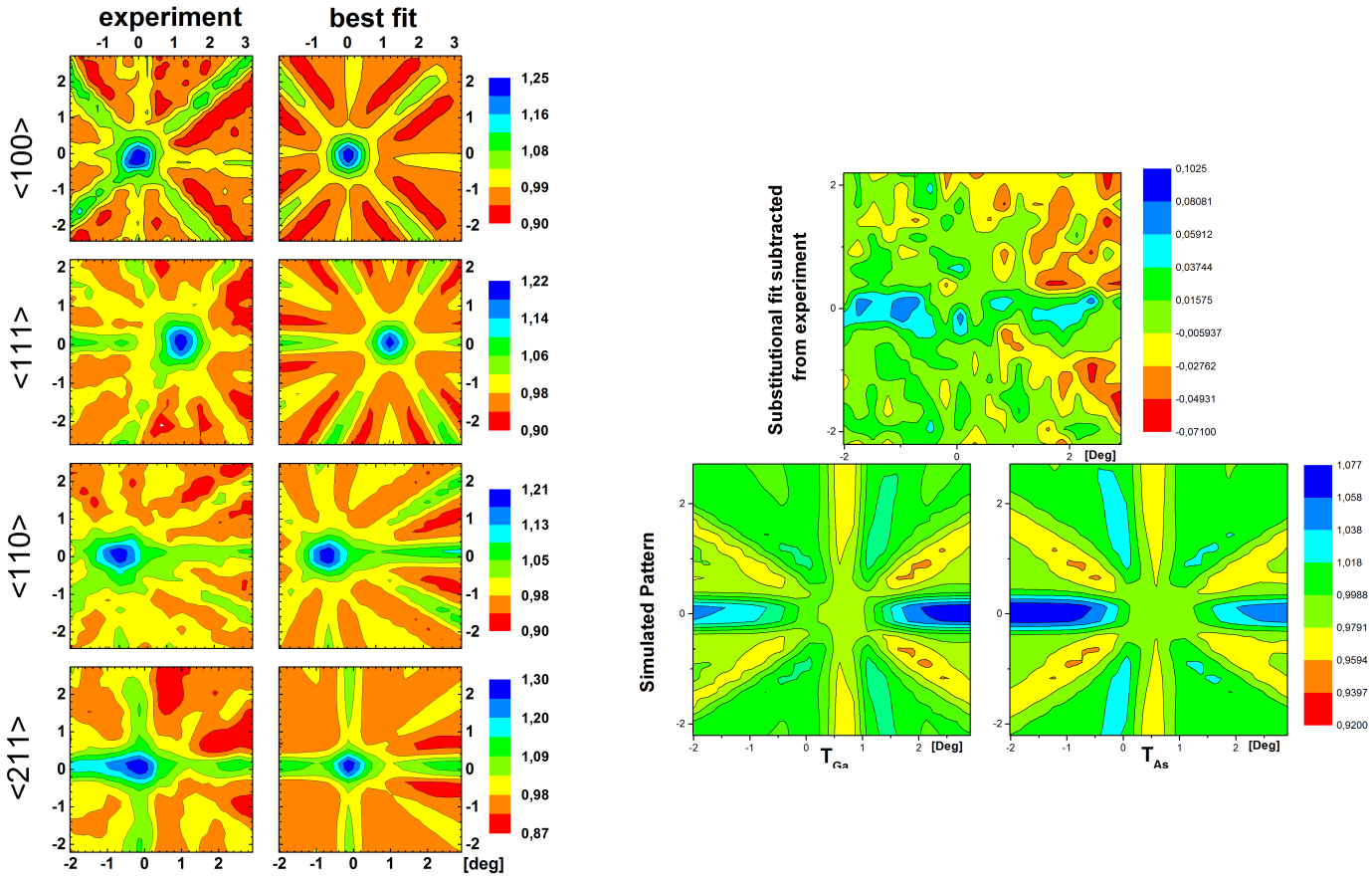


Figure 3.1: Experimental and fitted patterns for Mn implanted in GaMnAs in the as-implanted state on the left. On the right the fitted $S_{Ga}$ pattern subtracted from the experimental pattern is shown with the theoretical patterns for pure $T_{Ga}$ and pure $T_{As}$ site occupancy.

**Annealing kinetics**

With the lattice sites determined to be $S_{Ga}$ and $T_{As}$ we can proceed to study the evolution of the fractions with annealing temperature. Before proceeding with the interpretation of the data the so-called random fraction introduced in section 2.2.4 needs to be explained in terms of the process of dechanneling. Dechanneling can occur for several reasons at constant temperature, if the crystal is of low quality or implantation damage occurred, the crystallinity will be lower which will decrease the channeling since the necessary structure is lacking. The presence of secondary phases such as precipitates will also lead to dechanneling, as the crystal structure or composition is different, both affecting the channeling.

If the temperature is increased, the diffusion of the radioactive probe atoms will also lead to dechanneling. Diffusion into the bulk will lead to dechanneling since the scattering probability for the emitted electron increases with distance traversed. Conversely, if the probe atoms reach the surface the $\beta^-$ electrons will be emitted isotropically adding only to the random fraction.

The resulting fractions of substitutional and interstitial Mn for each annealing temperature are shown in figure 3.2. The results of three different experiments are plotted, 1% and 5% (GaMn)As data is taken from earlier work by Lima et al. [58], the 4% II-PLM (GaMn)As is the sample studied in this thesis.
From the graph one notices an increase in substitutional fraction as the annealing temperature is increased up to $150-200^\circ$ C. For the MBE samples no corresponding decrease in interstitial Mn is observed. Hence, rather than attributing the increase in $S_{Ga}$ fraction of the MBE samples to conversion of $Mn_{int}$ to $Mn_{sub}$ it is attributed to damage recovery during annealing. $Mn_{sub}$ present in formerly highly disordered regions will, after recrystallisation, contribute to the emission pattern and an increase in the measured fraction.
For the II-PLM sample this unambiguous attribution to damage recovery cannot be made since already after the first annealing step the interstitial fraction is lowered. However, considering the behaviour of the MBE samples - which differ from the II-PLM samples only in electrically active $Mn_{Ga}$- the increase in observed $Mn_{Ga}$ fraction is taken to be the result of damage recovery in the same manner as for the MBE samples.
At the other end of the temperature range, starting from 250°C for the 5% sample to 400°C for the 1% sample a significant decrease in $Mn_{Ga}$ fraction is observed. Since in this temperature range GaAs is far from degrading structurally ($T_m = 1240$°C), this decrease cannot be attributed to loss of crystalline quality and is the result of $Mn_{Ga}$ migrating out of its lattice location until it does not contribute to the emission pattern. For the decrease in $Mn_{int}$ at lower temperatures the same reasoning can be applied.

Aside from the increase in substitutional fraction after the first annealing step due to increase in crystallinity, all other changes in fractions are considered to be due to diffusion through the crystal. The current understanding is that $Mn_{int}$ diffuses towards the surface where it is passivated (for example by oxygen) or diffuses into the bulk towards the boundary with GaAs.[59] At higher temperatures, $Mn_{sub}$ will segregate and form clusters[60][58]. The change in fractions, which are caused by dechanneling either by movement towards to the surface or incorporation in a cluster, are thus seen to be related to the diffusion of Mn.

Before analysing these changes in the framework of diffusion models the different observations that are to be explained will be considered. Firstly, the dependence on concentration of the substitutional diffusion: as the concentration of Mn in the (GaMn)As sample is increased, the temperature at which $Mn_{Ga}$ starts to diffuse lowers. Secondly, the large difference in the interstitial and substitutional diffusion temperature, and lastly, the anomalously low diffusion temperature of $Mn_{int}$ for the II-PLM sample compared to the MBE samples, despite having a concentration between the two.

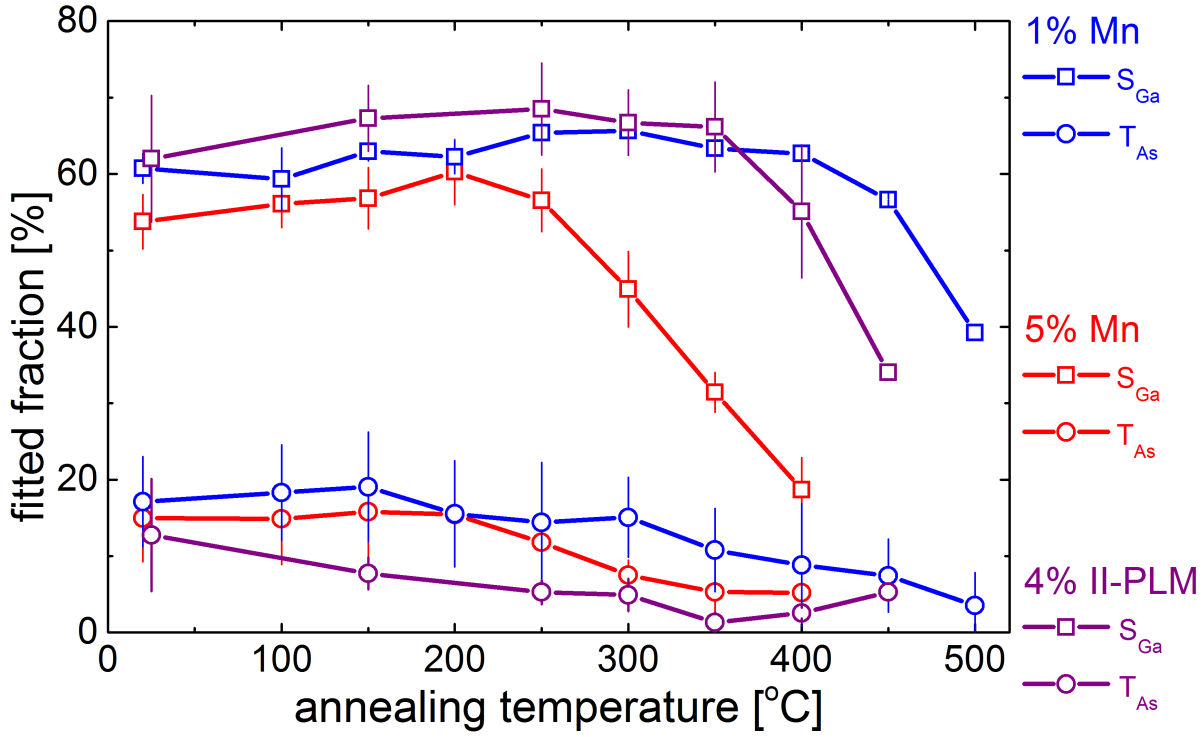


Figure 3.2: Fractions of implanted Mn present in either the $S_{Ga}$ and $T_{As}$ lattice location for two MBE samples and an II-PLM sample of respectively 1 %, 5% and 4% impurity concentration. The data for the MBE samples was taken from previous work by Lima et al. [58]

### 3.1.3 Diffusion of substitutional and interstitial Mn

#### Arrhenius model of thermal activation

Since the diffusion of Mn is a thermally activated process, it can be described by an Arrhenius model where the change in fraction (f) of Mn on its lattice location after an annealing time t at temperature T is described by:

$$\frac{f(T,t)}{dt} = -\frac{\nu f}{J} \tag{3.1}$$

Here J is the average amount of jumps the Mn atom has to make before it does not contribute to the emission yield any longer, either by diffusing too deep into the bulk, diffusing towards the surface or being incorporated in a secondary phase or low crystallinity region. Note that even if a Mn atom has jumped several times already (i.e. in the process of diffusing), as long as it remains in the equivalent lattice site while doing so it is not measured as having diffused.
The jump frequency $\nu$ is of the order of the lattice vibrations and hence depends on the temperature. For a given temperature (thermal energy) the jump frequency is then, based on the Boltzmann distribution, given by:

$$\nu = \nu_0 \exp\left[\frac{-E_a}{k_b T}\right] \tag{3.2}$$

where $\nu_0$ is taken to be $10^{12} s^{-1}$, on the same order as the lattice vibrations, $E_a$ is the activation energy and $k_b$ is the Boltzmann constant. Putting this in equation 3.1.3 and solving the differential equation one finds for the fraction at a given temperature T and after an annealing time t:

$$f(T,t) = f_0 \exp\left[(\frac{-\nu t}{J}) \exp(-\frac{E_a}{k_b T})\right]$$

In order to compare with theoretical calculations and other experiments, such as those done on the aforementioned MBE samples, the activation energy needs to be known. For the determination of the activation energies, $f$ is taken to be half of $f_0$ and t the corresponding annealing time to reach half of the original fraction. This leads to the following expression:

$$E_a = -k_b T \ln(\frac{J \ln(2)}{\nu_0 t}). \tag{3.3}$$

Since the exact temperature at which the fraction of Mn on a given lattice site is halved

is not known, a temperature range is considered which will lead to a range of possible activation energies. This equation contains two unknowns, the activation energy and the amount of jumps the diffusing Mn atom has to make before it is immobilized. The latter can be estimated by considering what constitutes a jump for respectively interstitial and substitutional Mn and knowing the distance a Mn atom has to travel before it does not contribute to the emission yield any longer.

### Interstitial diffusion mechanism

Interstitial diffusion is a very common diffusion mechanism whereby an interstitial atom jumps from interstitial to interstitial site throughout the crystal. For $Mn_{int}$ uncoordinated by $Mn_{sub}$ atoms this is indeed the case and the amount of jumps a Mn atom has to perform before being immobilised is much too large to consider as a discrete process. Hence it is usually modelled by Fick's law, assuming a continuous concentration gradient (or, more accurately, a gradient of chemical potential).
However, at the concentrations studied in this work and the earlier work by Lima et al. [58], this will not be the case and significant fractions of $Mn_{int}$ will be present in doublet $Mn_{int}$-$Mn_{sub}$ and triplet $Mn_{sub}$-$Mn_{int}$-$Mn_{sub}$ complexes. In this case the activation energy will consist of two terms: a migration energy ($E_m$) to jump to an interstitial site, and a binding energy ($E_b$) with the Mn atoms in the complex:

$$E_a = E_m + E_b$$

Because of this binding energy the activation energy of $Mn_{int}$ will be higher in a complex compared to free interstitial Mn. One can thus expect the dissociation of $Mn_{int}$ to happen at a much longer timescale than the movement between interstitial sites. As the (positively charged) $Mn_{int}$ travels through the crystal it will experience an attractive coulomb force to the negatively charged $Mn_{sub}$ atoms and once it enters their capture radius will be trapped and form a complex. The prevalence of $Mn_{int}$ in complexes thus changes the diffusion mechanism from a free interstitial diffusion process to a trap-limited diffusion. In this case it does make sense to model this as a discrete, random walk since the amount of jumps is given by the average amount of complexes in the path of the $Mn_{int}$ atom until it does not contribute to the interstitial fraction anymore.

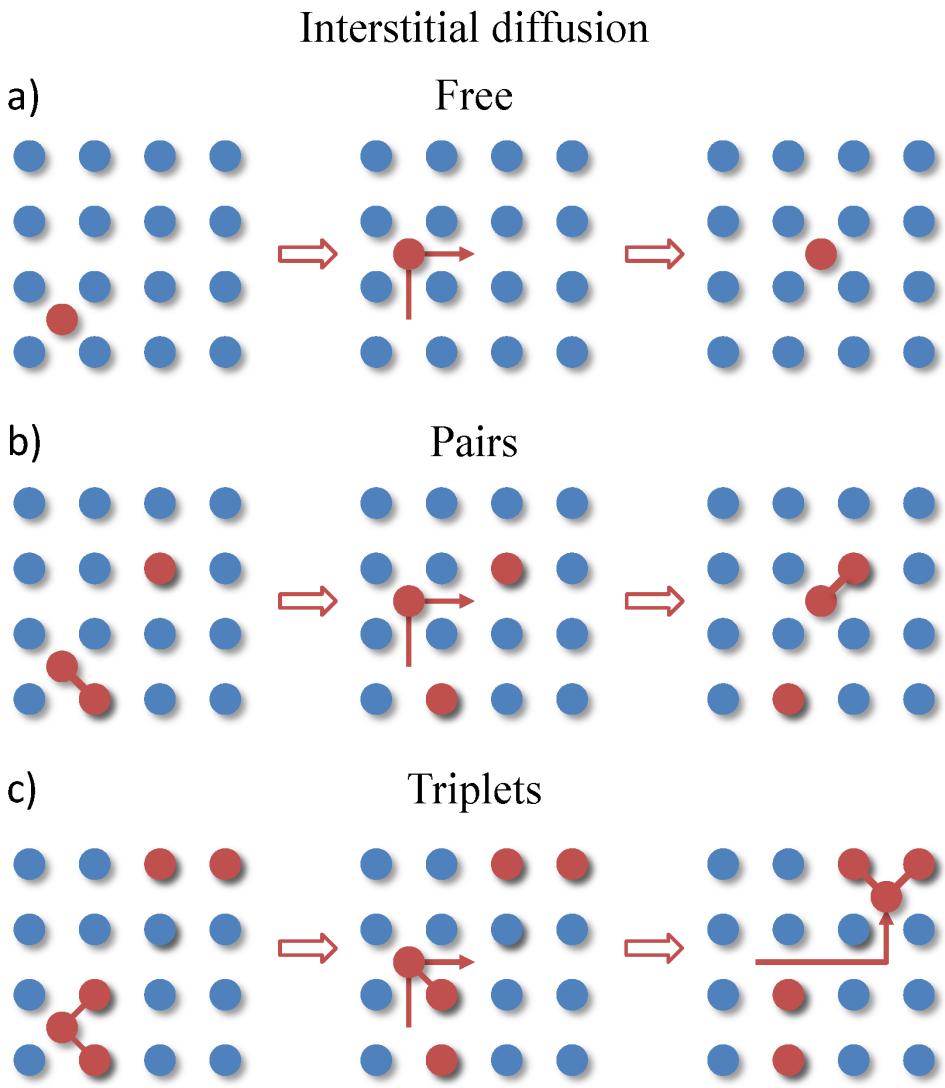


Figure 3.3: Different interstitial diffusion mechanism for different Mn complexes. The diffusion mechanism for free $Mn_{int}$ is qualitatively different from the mechanism for $Mn_{int}$ present in pairs or triplets, the latter being trap-limited diffusion. When trap-limited, the number of jumps (J) is given by the number of complexes $Mn_{int}$ goes through before being immobilized.

### Estimation of random jumps

To calculate the amount of jumps, the average distance traversed, the prevalence of the complexes and the average distance between them, needs to be known. An estimate for the fractions of $Mn_{sub}$ present in isolation or in pairs, assuming a random distribution of impurities, can be obtained from [61]. These are then available to form either doublet or triplet complexes with $Mn_{int}$ as it diffuses. The fractions of Mn forming pair and triplet complexes are respectively:

$$\begin{aligned} x_{pairs} &= (1-x)^{12} \\ x_{triplets} &= 12x(1-x)^{18} \end{aligned}$$

here x is the fraction of impurities. The distance between complexes is then estimated as:

$$d_i = \sqrt[3]{\frac{1}{c_{Mn}x_i}}$$

where i stands for the type of complex and $c_{Mn}$ is the concentration of Mn. For a three dimensional random walk the root mean square (rms) distance from the starting point after J jumps is given by:

$$\sigma_{(i,3)} = \sqrt{\langle r^2 \rangle} = \sqrt{J} d_i$$

As in the diffusion model only steps in the z-direction are considered -either towards the surface or into the bulk- only one third of the jumps will contribute to the diffusion process:

$$\sigma_{(i,1)} = \sqrt{\frac{J}{3}} d_i$$

During the emission channeling experiments the probe atoms are implanted as a gaussian depth profile. The average distance the Mn atoms have to traverse to reach the surface (or diffuse into the bulk) is then taken to be the projected range $R_p$. The number of jumps for each diffusion scenario is then approximately given by:

$$J \approx 3\left(\frac{R_p}{d_i}\right)^2$$

This can then be used as input in the Arrhenius model described in section 3.1.3 to estimate the activation energy for each scenario. Of course a given diffusing Mn atom will encounter a mixture of triplet and doublet complexes and the real activation energy will lie in the range given by the activation energies for the different scenarios. Free interstitial

diffusion is not considered since at these impurity concentrations every $Mn_{int}$ is considered to encounter, and become trapped by, complexes.

### Interstitial activation energy

Having calculated the amount of jumps for each different scenario (diffusion between either doublets or triplets) ,the activation energies can be calculated. The calculated activation energies are listed in table 3.1.

| % Mn | $T_D$ [°C] | $E_a$[eV] pairs | $E_a$[eV] triplets |
|---|---|---|---|
| 1 | 500-550 | 1.5-1.7 | 1.6-1.8 |
| 4 (II-PLM) | 150-250 | 1.0-1.2 | 0.9-1.2 |
| 5 | 350-400 | 1.3-1.5 | 1.3-1.5 |

Table 3.1: Estimated activation energies for $Mn_{int}$. Data for the 1% and 5% samples are taken from [58].

As expected from the diffusion temperature these activation energies do not follow the concentration in a monotonous way. Another factor, distinguishing the II-PLM sample from the MBE samples is at play. We do not expect either from the sample preparation, or the diffusion temperatures for $Mn_{sub}$, that the real concentration differs from the nominal concentration as the substitutional diffusion does have a monotonous dependence on the concentration. However, the II-PLM sample has a non-trivial depth profile [48] resembling more closely a gaussian implantation profile. The sample interstitial Mn fraction (not implanted during EC) should be very low and hence the electrically active Mn distribution should follow this gaussian profile as well.

As early as 1958 the effect of an internal electric field due to the doped charge carriers in semiconductors was investigated.[62] Since the charge carriers are much more mobile than the substitutional impurity atoms at the relevant diffusion temperature an equilibrium charge carrier distribution will form which will not necessarily be constant as a function of depth. This hole gradient will lead to a built-in electric field which will affect the diffusion of charged impurities. More recently this built-in electric field was considered in (Ga,Mn)As by L. Horák in 2011[63] and Proselkov et al. in 2012.[64]. Both found a hole gradient in the sample based on a theoretical solution of the diffusion-drift equations:

$$\begin{aligned}\frac{dMn}{dt} &= \frac{d}{dz}\left[D_{Mn}\frac{dMn}{dz} + \mu_{Mn}Mn\frac{d\phi}{dz}\right] = \frac{d}{dz}(-j_{Mn}) \\ \frac{dp}{dt} &= \frac{d}{dz}\left[D_p\frac{dp}{dz} + \mu_p p\frac{d\phi}{dz}\right] = \frac{d}{dz}(-j_p)\end{aligned}$$

where Mn and p stand for the density of intersititials and holes respectively, $D_{Mn}$ and $D_p$ are their respective diffusion constants related to the mobility by the Einstein relation and $\phi$ is the electrostatic potential. Poisson's equation has to be fulfilled as well:

$$\frac{d^2\phi}{dz^2} = (c_{sub} - p - 2Mn)\frac{e}{\epsilon} \tag{3.4}$$

where $c_{sub}$ is the fraction of substitutional Mn atoms and the factor 2 in front of the $Mn_{int}$ concentration is because it is a double donor and when fully ionised, positively charged. Using the correct boundary conditions and taking into account the oxidation at the surface of interstititial Mn which releases two holes, this system can be solved for hole and interstitial Mn concentration. Both papers found a negative hole gradient into the bulk leading to an electric field which improves the out-diffusion of interstitial Mn. We hypothesise that it is this electric field which causes the anomalously low activation energy of $Mn_{int}$ for the II-PLM sample and lowers the activation energy of the 5% sample compared to the 1% sample. The activation energy of $Mn_{int}$ equals: $E_a = E_m + E_b$. The binding energy can be assumed to be constant for a given complex regardless of impurity concentration since it depends mostly on the atomic species involved. The migration energy however, will be lowered due to the electric field present in the (Ga,Mn)As thin film. The difference in activation energy between the 1% and 5% sample is then readily explained by the higher hole concentration in the 5% sample causing a higher electric field. For the II-PLM sample the large gradient is the result of the physical gradient in the depth profile of the electrically active $Mn_{sub}$ atoms in the film. This results in a similarly large gradient in the hole concentration which one expects to be much larger compared to the MBE samples with a constant $Mn_{sub}$ depth profile.

### Substitutional diffusion mechanism and activation energy

At higher temperatures than $Mn_{int}$, $Mn_{sub}$ starts to diffuse. This results in the generally accepted phase segregation and clustering leading to the decrease in Curie temperature at higher annealing temperatures. The usual mechanism for substitutional diffusion is (oxymoronically named) vacancy diffusion whereby a substitutional atom jumps out of its lattice site into a nearby vacancy. However, two conditions are met which imply that the dominant diffusion mechanism for $Mn_{sub}$ is the Frank-Turnbull dissocation mechanism.[65] These two conditions are: (1) Substitutional atoms and interstitial atoms are both present and the substitutional to interstitial ratio is much larger than unity. (2) The diffusivity of interstitials is much larger than the diffusivity of substitutional atoms, so that the substitutional atoms can be considered immobile.

Frank-Turnbull diffusion has $Mn_{sub}$ jumping out of its lattice site (the dissociation) leaving behind a vacancy on the gallium site ($V_{Ga}$). It will then diffuse as interstitial atom much more rapidly and eventually recombine with a gallium vacancy. This will continue until the Mn atom reaches a Mn complex or cluster. Since the interstitial diffusion is so much larger at this temperature the amount of jumps before $Mn_{sub}$ is immobilised is taken to be 1.

Given the temperature range at which the $Mn_{sub}$ fraction is halved and using $J = 1$ the activation energy is readily calculated. The calculated activation energy for the II-PLM sample and the earlier results on the MBE samples are shown in table 3.2 .

| % Mn | $T_D$ [°C] | $E_a$[eV] |
|---|---|---|
| 1 | 500-550 | 2.3-2.6 |
| 4 (II-PLM) | 450 | 2.1 |
| 5 | 350-400 | 1.9-2.0 |

Table 3.2: Estimated activation energies for $Mn_{Ga}$. Data for the 1% and 5% sample is taken from [58].

As expected from the data, lower activation energies are found for $Mn_{Ga}$ at higher impurity concentrations. The result for the II-PLM sample, together with the results on the MBE samples, imply that the diffusion behaviour of $Mn_{Ga}$ depends mainly on the concentration. A model explaining this behaviour is put forward in the following section.

### Percolation-cluster diffusion

The dependence of the activation energy on the concentration seems counter-intuitive since for each concentration the amount of jumps is 1 and the binding energy of an isolated $Mn_{sub}$-$V_{Ga}$ complex remains the same. However at such high impurity concentrations ($\approx 8 \cdot 10^{20} cm^{-3}$) the $Mn_{sub}$ atoms cannot be considered independent of each other. In this regime a model was was proposed by D. Mathiot and J. Pfister in 1984 which combines normal vacancy/interstitial-assisted diffusion and diffusion in a percolation cluster formed by the substitutional impurity atoms[66]. In 1993, A. Larsen et al. used the same model to describe the unexpected change in diffusivity for impurities in heavily doped silicon. They argued that at impurity concentrations higher than $\approx 2 \cdot 10^{20} cm^{-3}$ collective phenomena, as modelled in a vacancy-percolation cluster, start dominating.[67]
More explicitly, once a substitutional Mn atom jumps out of its lattice site and leaves a vacancy behind one considers a diffusion step to be complete once the vacancy diffuses to, say, the third nearest neighbour. Once the concentration is high enough that another $Mn_{sub}$ atom is present at the fifth-nearest neighbour, then the third nearest neighbour

position to which the vacancy has to diffuse will also be the second-nearest position to the other $Mn_{sub}$ atom. This will lower the binding energy of the original $Mn_{sub}$-$V_{Ga}$ complex by an energy $\Delta E$ equal to the binding energy between the vacancy and the second $Mn_{sub}$ atom. In this way a percolation cluster will form wherein the vacancies have a lowered binding energy and will diffuse more easily. This then improves the diffusion of the $Mn_{sub}$ atoms as well by a simple vacancy exchange mechanism.

We hypothesise that it is this mechanism which causes the decrease in activation energy for $Mn_{sub}$ with increasing impurity concentration. By reducing the distance between $Mn_{sub}$ atoms the binding energy of the $Mn_{sub}$-$V_{Ga}$ complex is decreased since the vacancy is attracted to the other surrounding $Mn_{sub}$ atoms.

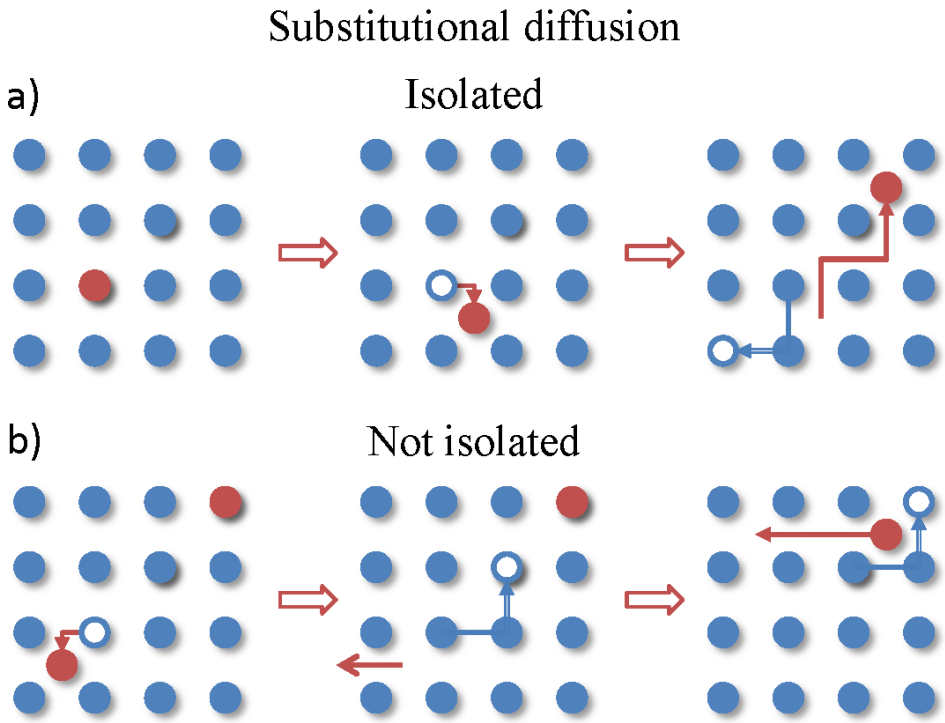


Figure 3.4: Frank-Turnbull diffusion for substitutional Mn. The presence of other Mn atoms at high concentrations causes the binding energy of the $Mn_{sub}$-$V_{Ga}$ complex to lower which lowers the activation energy for the $Mn_{sub}$ to diffuse.

### 3.1.4 Conclusion

As was shown in earlier work by Lima et al.[58] the thermal stability of Mn in (Ga,Mn)As is impurity concentration dependent. For substitutional Mn this dependence is monotononic on the impurity concentration and a mechanism based on vacancy diffusion in a percolation cluster is shown to explain this behaviour. For interstitial Mn the activation energies did not show a monotonous dependence on impurity concentration with the II-PLM sample having an anomalously low activation energy compared to the MBE samples. This was explained to be the result of an in-built electric field caused by a non-constant hole depth profile. The interstitial activation energy is thus only indirectly related to the impurity concentration, either by the concentration of electrically active $Mn_{sub}$ donating holes, or a gradient in the depth distribution of $Mn_{sub}$ as in the case of the II-PLM sample. We are currently performing scanning spreading resistance microscopy measurements (SSRM) which will provide a quantitative profile of the charge carrier distribution in the II-PLM (Ga,Mn)As film.

## 3.2 GaN

### 3.2.1 Summary of earlier work

Because of the chemical similarities one expects transition metals (Mn, Fe, Co, Ni) to occupy the cation site in GaN and the similar wide-gap semiconductor ZnO. This was indeed confirmed by several X-ray absorption fine structure (XAFS) and ion-channeling experiments and found to be independent of growth method (during growth, ion implantation).[38][12][68][69][70] Recent emission channeling experiments performed by Pereira et al. on GaN and ZnO found that aside from the cation substitutional fraction also an anion substitutional fraction was present for certain combinations of host and transition metal (TM). For wurtzite GaN, a minority anion fraction was observed for implanted Mn and Co and in wurtzite ZnO minority substitution was found by Mn, Ni and Co.[40][71] This came as a challenge to the accepted understanding of the transition metal implanted DMS GaN and ZnO and therefore theoretical considerations of the anion substitution are scarce.

In a recent paper by Pereira et al. a mechanism was proposed that would explain the observed dependency of anion substitution on host-transition metal pair.[71] For anion substitution to occur the formation energy of the defect should be small. Since anion substitution was not considered in the literature before, the defects that resemble them the most were considered: the cation antisite defects. Of these defects it has been shown

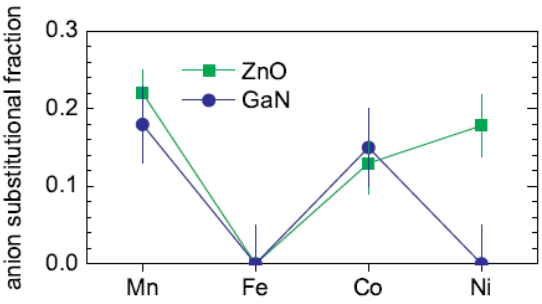


Figure 3.5: Fraction of anion-substituted implanted Mn, Ni, Co and Fe in dilute magnetic semiconductors GaN and ZnO in the as-implanted state. Taken from [71]

that depending on the growth conditions (availability of Ga and Zn atoms) the 4+ charge state can be stable with the 3+/4+ and 2+/3+ transition levels deep in the bandgap. Under metal-rich growth conditions and the fermi level close to the valence band maximum (VBM) the formation energy was shown to be small or even negative.[72] At first sight this result cannot be extrapolated to TM anion substitution since the four TM's have open 3d shells whereas Zn and Ga do not. However in the stable 4+ anion antisite state both Zn and Ga have open 3d shells, making them similar to the TM's in both ionic radius and electron configuration. Hence one expects the anion substitution of the TM's to be qualitatively similar to the cation antisite defect except for an energy shift in the 1+/2+/3+/4+ transition levels. From these considerations two conditions were proposed for TM anion substitution:

**N-or O-poor conditions** during growth, or equivalently, the presence of N and O vacancies. The presence of the anion vacancies are necessary for the TM substitution or filling of the vacancy. In emission channeling these vacancies are in principle generated during ion implantation of the TM probe.

**Fermi level position** under the 3+/4+ transition level of the TM substituted anion site. For the defect to be stable in the 4+ charge state with low formation energy enough acceptor states have to be present. These could be supplied by the TM present on the cation site with deep transition level 2+/3+ in GaN. Another possibility is that the Fermi level position is set by the presence of electrically active defects. This could be either wanted defects, such as introduced by electrical doping or defects generated during implantation. This condition would explain the observed non-monotonous dependence on transition metal of the anion substitution since the 2+/3+ cation charge state level was calculated to depend non-monotonously on the atomic number of the TM defect [73]. Since the anion 3+/4+ charge transfer level and the Fermi level depend on the host semiconductor this would also explain why anion substitution is observed for Ni implanted

ZnO whereas no anion occupancy is found for Ni implanted GaN.

A last result in the same paper was an observed displacement of the $S_{Ga}$ site towards the anti bonding site along the c-axis for nickel implanted GaN. This was attributed to the presence of nitrogen vacancies generated during implantation. The amount of vacancies and defects generated during implantation is of the order of several hundreds per implanted ion. Even taking spontaneous recombination into account one can assume the amount of vacancies present to form complexes with the nickel atoms is of the same order.

The observed displacement can then be explained as being caused by the repulsive interaction between the positively charged $Ni_{Ga}$ cation and a positively charged nearest neighbour nitrogen vacancy. It has been shown in several ab-initio calculations that the nitrogen vacancy is present in the positive single ionised charge state for (naturally ) n-type GaN and in the positive triple-ionised charge state for p-type GaN. However it is also predicted that if the Fermi level is raised enough (n-type charge carrier concentration of $10^{19} cm^{-3}$) the $V_n^-$ vacancy becomes favorable.[74] It could then be possible to switch the cation displacement towards the bonding site if indeed the nitrogen vacancy is responsible for this.

### 3.2.2 GaMnN

#### Experimental Details

An (Ga,Mn)N sample of 2.5 % impurity concentration was implanted with radioactive $^{56}$Mn ($T_{1/2}$ = 2.56 hours) probe atoms at an angle of 17° to the (0001) surface to minimize ion channeling. An implantation energy of 40 keV was used, resulting in a depth profile centered around a projected range of 242 Å with a straggle of 129 Å . After implantation, measurements were made with the sample at room-temperature, and annealed to 300°C, 500°C, 700°C, 800°C and 900°C. The measurements were made along the $\langle 0001 \rangle$ , $\langle \bar{1}101 \rangle$, $\langle \bar{1}102 \rangle$ and $\langle \bar{2}113 \rangle$ directions.

#### Results

First, a one-site fit was done for all high-symmetry lattice sites (see figure 1.3) in the GaN crystal. As in the analysis of the GaMnAs emission channeling experiment, measuring along the $\langle 0001 \rangle$ direction offers little information, not distinguishing between substitutional or interstitial Mn. However along the three other directions measured: $\langle \bar{1}101 \rangle$, $\langle \bar{1}102 \rangle$ and $\langle \bar{2}113 \rangle$, one can distinguish all high-symmetry locations and all three were used

in the full analysis. The best fit was obtained for $S_{Ga}$ as one would expect from comparing the ionic radii and electron structure of Mn and Ga. Also Mn and Ga are respectively a transition metal and a metal whereas N is a non-metal making anion-substitution less likely.

Moving on to a two-site fit model a host of second sites have to be considered. No significant fractions or fit improvements were found for any of the more exotic sites such as the SP, H or C sites. For the more common bond centered (BC), anti-bonding centered (AB) and tetrahedral (T) sites more care has to be taken since the analysis is complicated by the reduced symmetry of the crystal. Two directions can be distinguished in the wurtzite crystal structure, the c-axis direction and the basal direction. Along the c-axis (see figure 3.6) a clear improvement in the fit can be seen when the second site corresponds to a displaced site towards the Gallium anti-bonding site ($AB_{Ga}$). Two other lattice sites also show a fit improvement, $AB_{Ga}$ displaced towards the interstitial site and the displaced towards the BC site. The latter can be dismissed since only two out of three directions show an improvement and these two don't agree on the displacement. To exclude the former a three-site fit was made which contained the $S_{Ga}$ site, the $S_{Ga}$ displaced towards $AB_{Ga}$ site and $AB_{Ga}$ displaced towards T. With these three sites taken into account only negligible occupation ( $< 5\%$) of the displaced towards T site was found and hence this site was not considered in the final analysis.

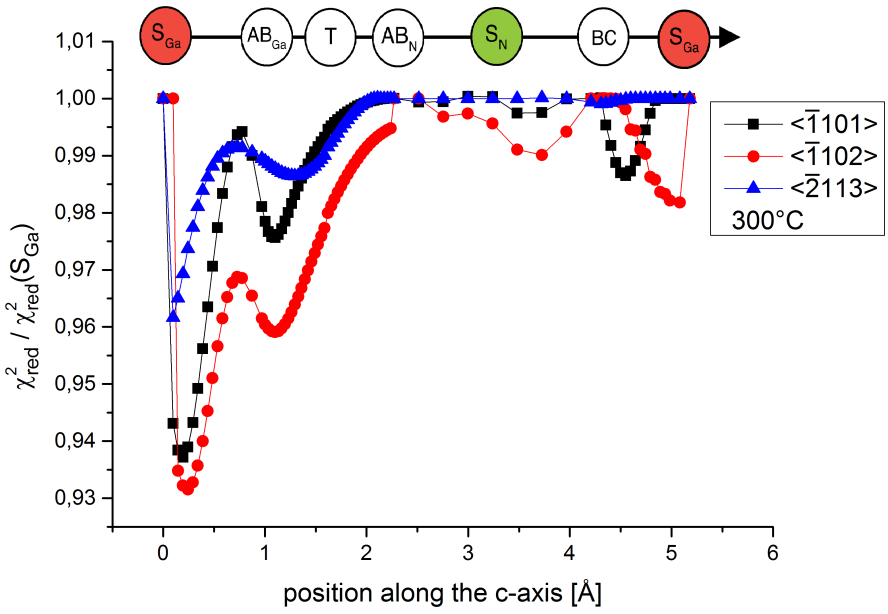


Figure 3.6: Reduced $\chi^2$ values of a two-site fit to the experimental emission yields as seen along the directions $\langle\bar{1}101\rangle$, $\langle\bar{1}102\rangle$ and $\langle\bar{2}113\rangle$ of Mn implanted GaMnN after a 300 °C annealing step. The sites under consideration are $S_{Ga}$ and as second site one of the high symmetry sites and displacements between them along the c-axis. All $\chi^2$ values were normalised to the $\chi^2$ value of the pure substitutional fit.

As mentioned before, the basal direction also needs to be considered and a two-site fit was made considering the bonding and anti-bonding sites and displacements in between them (see figure 3.7. Since a fit improvement for a $S_{Ga}$ displaced towards the $BC_{Ga}$(a) site could not be excluded, a three-site fit was considered containing the $S_{Ga}$ site, the displaced $AB_{Ga}$(c) site and the displaced $BC_{Ga}$(a) site. From this fit one can see that the measurement along the $\langle 2113 \rangle$ direction does not show an improvement and the measurement along the two other directions don't agree on the displacement. Hence any occupation of a basal direction site was taken to be negligible.

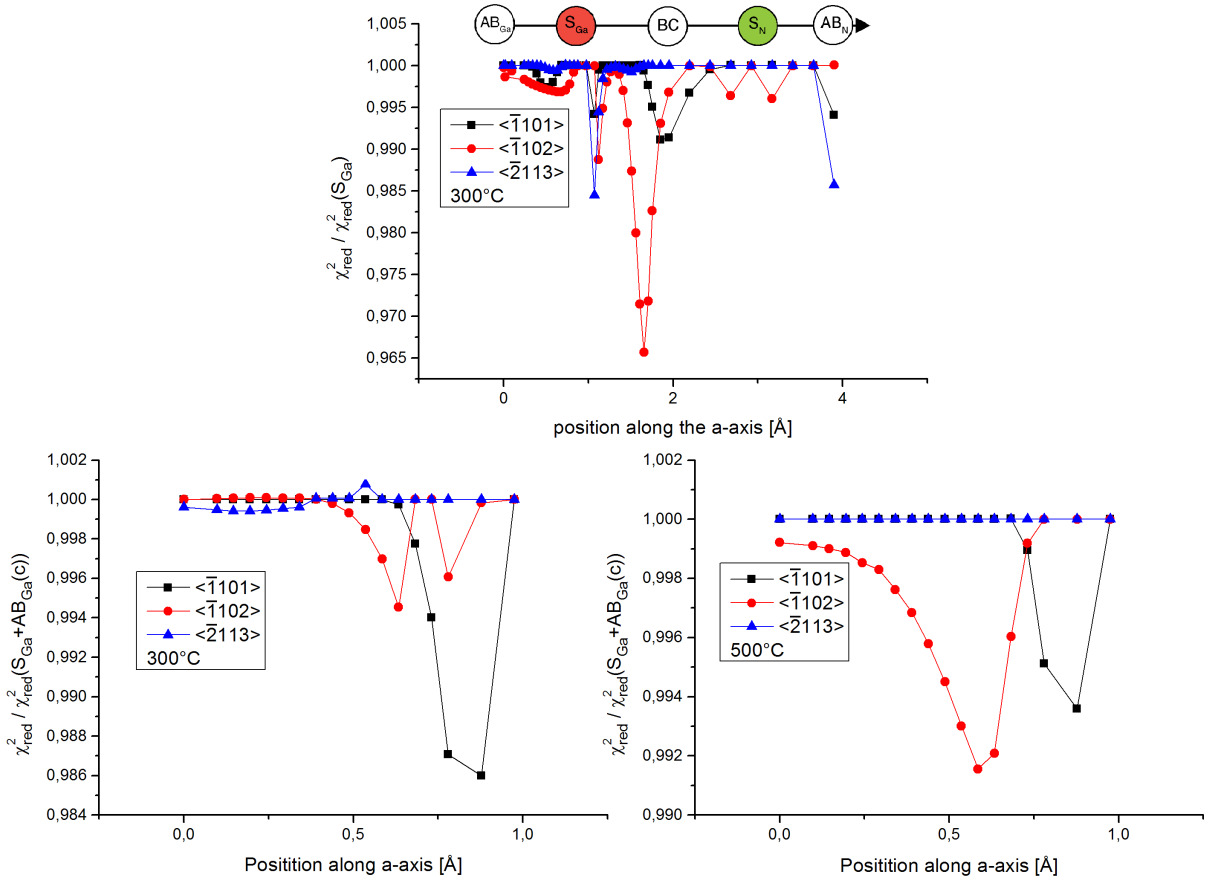


Figure 3.7: Reduced $\chi^2$ values of respectively a two-site fit and three-site fits to the experimental emission yields as seen along the directions $\langle \bar{1}101 \rangle$, $\langle \bar{1}102 \rangle$ and $\langle \bar{2}113 \rangle$ of Mn implanted GaMnN after a 300° C and 500 ° C annealing step. The sites under consideration are $S_{Ga}$ and as second site one of the high symmetry sites and displacements between them along the a-axis for the two-site fit. For the three-site fits containing $S_{Ga}$ and the $S_{Ga}$ displaced towards $AB_{Ga}$ site only lattice sites between $S_{Ga}$ and the BC site along the a-axis site were considered.

The final analysis was made with the $S_{Ga}$ site, and the $S_{Ga}$ displaced towards the $AB_{Ga}$

site. For the as-implanted sample a displacement of $0.17 \pm 0.08$Å was found and fractions of respectively $39 \pm 6\%$ and $27 \pm 8\%$ for the $S_{Ga}$ site and displaced site. The values for the whole temperature range have been plotted as part of figure 3.12. From this plot a slight conversion from the $S_{Ga}$ site to the displaced site can be seen. This would probably be related to the diffusion of nitrogen vacancies in the sample causing a more efficient $Mn_{Ga}$-$V_N$ formation but since this conversion is within error bars this is a tentative conclusion at best.

### 3.2.3 p-,n-GaN

#### Experimental Details

A p-type Mg doped GaN sample with a hole concentration of $2 \cdot 10^{17}$ cm$^{-3}$ and an n-type Si doped GaN sample with electron concentration of $1 \cdot 10^{17}$ cm$^{-3}$ were both implanted with radioactive $^{56}$Mn ($T_{1/2} = 2.56$ hours) probe atoms at an angle of 17° to the (0001) surface to minimize ion channeling. An implantation energy of 50 keV was used, resulting in a depth profile centered around a projected range of 420 Å with a straggle of 200 Å for the n-type doped GaN film and a a projected range of 415 Å with a straggle of 198 Å for p-typed doped GaN. After implantation, measurements were made with the sample at room-temperature, and annealed to 300°C, 600°C and 900°C. The measurements were made along the $\langle 0001 \rangle$ , $\langle \bar{1}101 \rangle$, $\langle \bar{1}102 \rangle$ and $\langle \bar{2}113 \rangle$ directions.

#### Results

To analyse the p- and n-type GaN the same libraries were used and since the experimental parameters were the same, all measured differences between them should be a result of the sample differences only. First a one-site fit was made for all high-symmetry sites and displacements between them. The results are shown in figure 3.8. Unexpectedly the best fit was found for a $S_{Ga}$ displaced towards the $AB_{Ga}$(c) site for both samples rather than the $S_{Ga}$ site. These displacements are small and resolving these displacements is at the limit of what the emission channeling technique is capable of. Hence a two-site fit was performed with undisplaced $S_{Ga}$ instead.

As can be seen from the reduced $\chi^2$ plot for the two-site fit (see figure 3.9), the displaced $AB_{Ga}$(c) site gives the best fit for second site occupancy. Two other possible sites for a three-site fit were identified as the $AB_{Ga}$(c) displaced towards T site and the BC site. However in a three-site fit both sites offered fractions at the limit of what can be resolved ( $< 7\%$). Hence for the remainder of the analysis the two-site fit model of a displacement towards the $AB_{Ga}$(c) site and $S_{Ga}$ site was used.

Already from the $\chi^2$ plots it is obvious that there is a large difference between directions, for instance the $\langle \bar{2}113 \rangle$ direction does not find any fit improvement for a BC site occupancy whereas the other two do. This difference is even more apparent when plotting the manganese fractions on $S_{Ga}$ and the displaced site for the different directions (see figure 3.10). Although the $\langle \bar{1}101 \rangle$ and $\langle \bar{1}102 \rangle$ directions agree on the displacement all three directions have large variations in site occupancy. On basis of these results it is very difficult to decide whether or not to exclude a direction for inconsistency. If there were

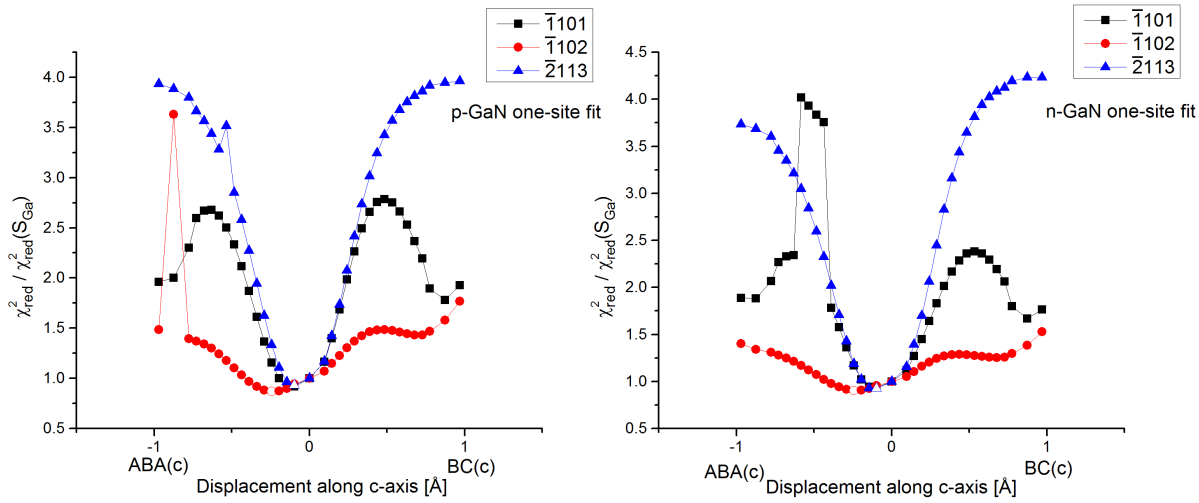


Figure 3.8: Reduced $\chi^2$ values of a one-site fit to the experimental emission yields as seen along the directions $\langle\bar{1}101\rangle$, $\langle\bar{1}102\rangle$ and $\langle\bar{2}113\rangle$ of Mn implanted p- and n-type GaN after a 300° C annealing step. The site under consideration is either $S_{Ga}$, BC and $AB_{Ga}$ site and displacements between them along the c-axis. All $\chi^2$ values were normalised to the $\chi^2$ value of $S_{Ga}$. The minimum in $chi^2$ for each direction is marked by an unfilled symbol. The minimum (i.e. the best fit) is found to be the displaced site towards $AB_{Ga}$ for both samples.

any diffusion or conversion between the sites, accurate knowledge of the site occupancy would be necessary. Since in this case for each direction there seems to be very little, if any, diffusion or conversion present, the lack of agreement between directions is not a great loss. The average fractions and displacements for each direction are shown in figure 3.12. As expected from the differences between directions the error on the fractions is very large. Still it's possible to be confident in the determination of the lattice sites since the displacement differs much less between directions with, for example, the implanted state having a displacement of $16 \pm 6\%$ and $18 \pm 7\%$ for p- and n-type GaN respectively. The fractions for $Mn_{Ga}$ and displaced $Mn_{Ga}$ as well as the displacement, as a function of temperature, can be found in figure 3.12.

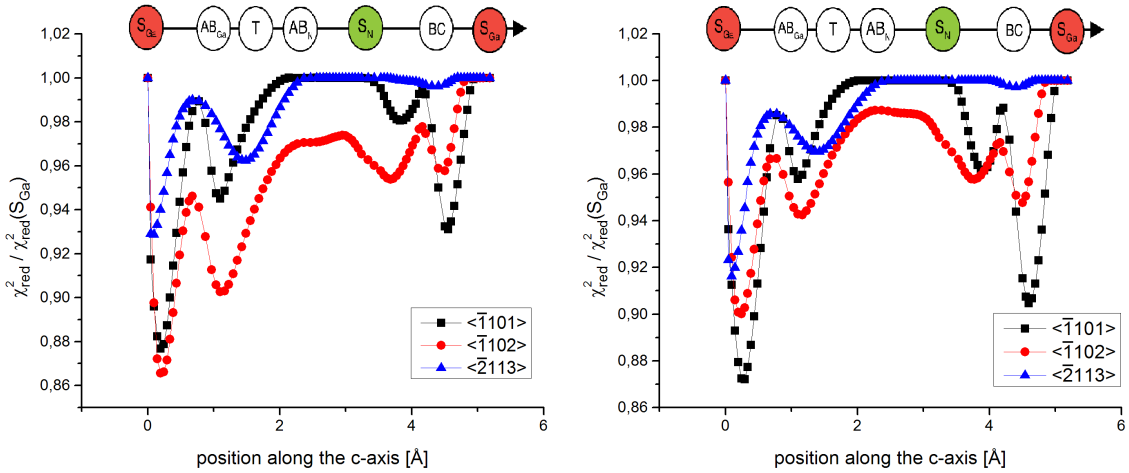


Figure 3.9: Reduced $\chi^2$ values of a two-site fit to the experimental emission yields as seen along the directions $\langle\bar{1}101\rangle$, $\langle\bar{1}102\rangle$ and $\langle\bar{2}113\rangle$ of Mn implanted p-(left) and n-type(right) GaN after a 300° C annealing step. The sites under consideration are $S_{Ga}$,and as second site a high symmetry site or displacements between them along the c-axis. All $\chi^2$ values were normalised to the $\chi^2$ value of $S_{Ga}$. The best fit is achieved with a displacement towards $AB_{Ga}$. The $AB_{Ga}$(c) displaced towards T and the BC site could possibly also be occupied but are excluded on basis of a three-site fit.

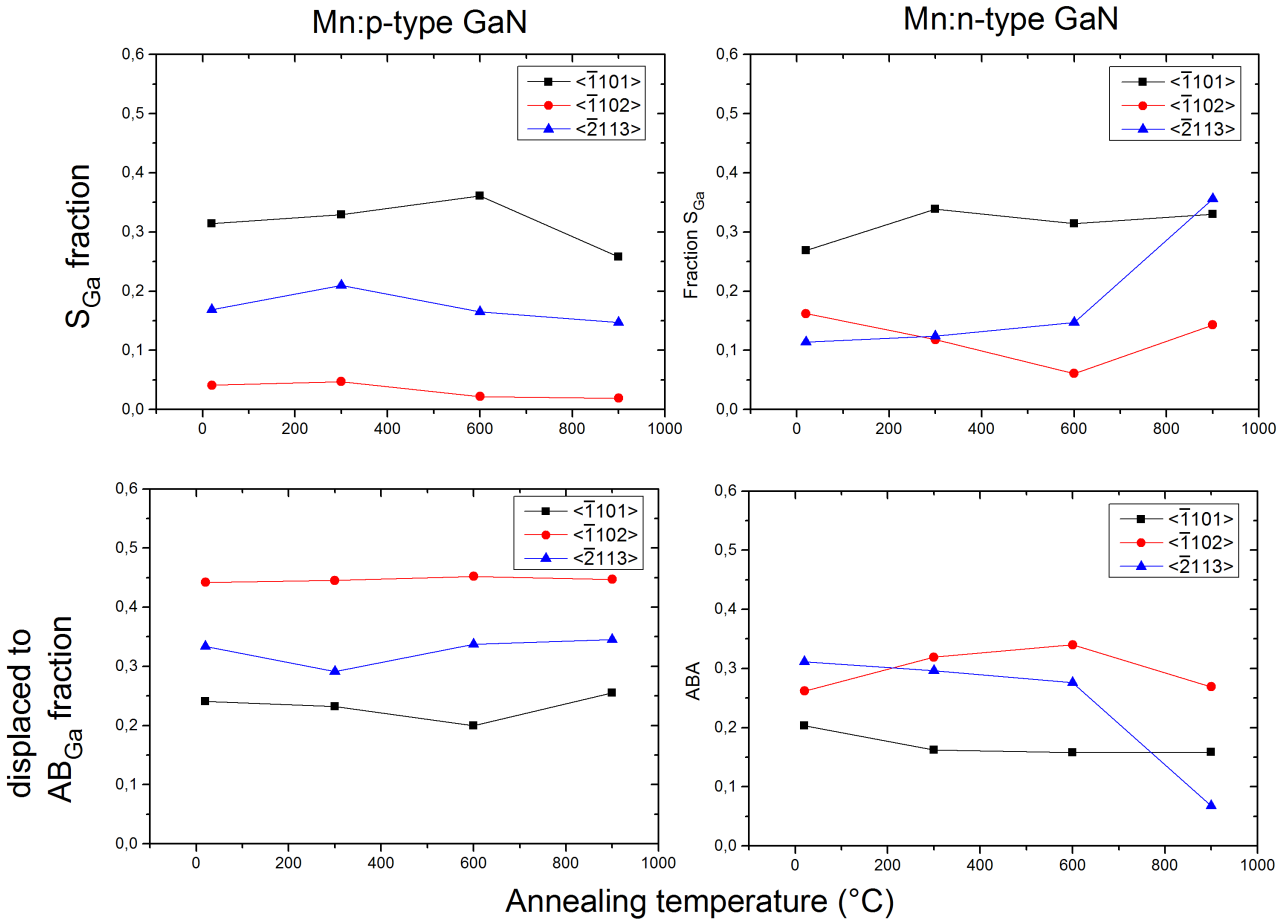


Figure 3.10: $S_{Ga}$ and $S_{Ga}$ displaced towards the $AB_{Ga}$ site fractions for Mn implanted p- and n-type GaN at an annealing temperature of 300 ° C for the three directions $\langle\bar{1}101\rangle$, $\langle\bar{1}102\rangle$ and $\langle\bar{2}113\rangle$. Note that although there is a large discrepancy between the directions, the sum of $S_{Ga}$ and the displaced fraction sum to more or less same value for all three directions.

### 3.2.4 Fe:GaN

For the purpose of comparison with a different TM dopant an old dataset on Fe implanted GaN [75] has been re-analysed.

#### Experimental Details

A commercially grown GaN film of 1-2 micron thick was implanted with the precursor isotope $^{59}$Mn at an energy of 60 keV. This isotope decays to the radiactive isotope $^{59}$Fe. During the decay $^{59}$Fe receives a nuclear recoil of about 200 eV, ensuring that its lattice location is unrelated to the lattice location of implanted Mn. The measurements were made at room-temperature, from 200°C to 800°C in steps of 200°C, and 900°C and along the $\langle 0001 \rangle$ , $\langle \bar{1}101 \rangle$, $\langle \bar{1}102 \rangle$ and $\langle \bar{2}113 \rangle$ directions.

#### Results

Since the only difference with the earlier obtained results by Wahl[75] and Pereira[71]- who found only $S_{Ga}$ and $S_{Ga}$+displaced $AB_{Ga}$ sites respectively- are updated simulation libraries, no large differences are to be expected. Unsurprisingly then, a one-site fit model finds the $S_{Ga}$ site as best fit. Adding a second site to be fitted finds no significant improvement, except for possible displacements between $S_{Ga}$ and the BC or $AB_{Ga}$ sites (see figure 3.11). The best fit is obtained for all three directions with the displacement towards $AB_{Ga}$ added as found before by Pereira. However it isn't possible to completely rule out that a fraction could also occupy a near BC site. As its presence can neither be excluded or confirmed, for simplicity the two-site fit with displacement towards $AB_{Ga}$ was used as it offers the best agreement in general. The average fractions and displacement found are plotted in figure 3.12. The increase in $S_{Ga}$ fraction after annealing at 200°C is related to damage recovery and at higher annealing steps no large change in fraction is found implying no diffusion takes place. The fractions of $Fe_{Ga}$ and displaced $Fe_{Ga}$ and the displacement as a function of temperature can be found in figure 3.12.

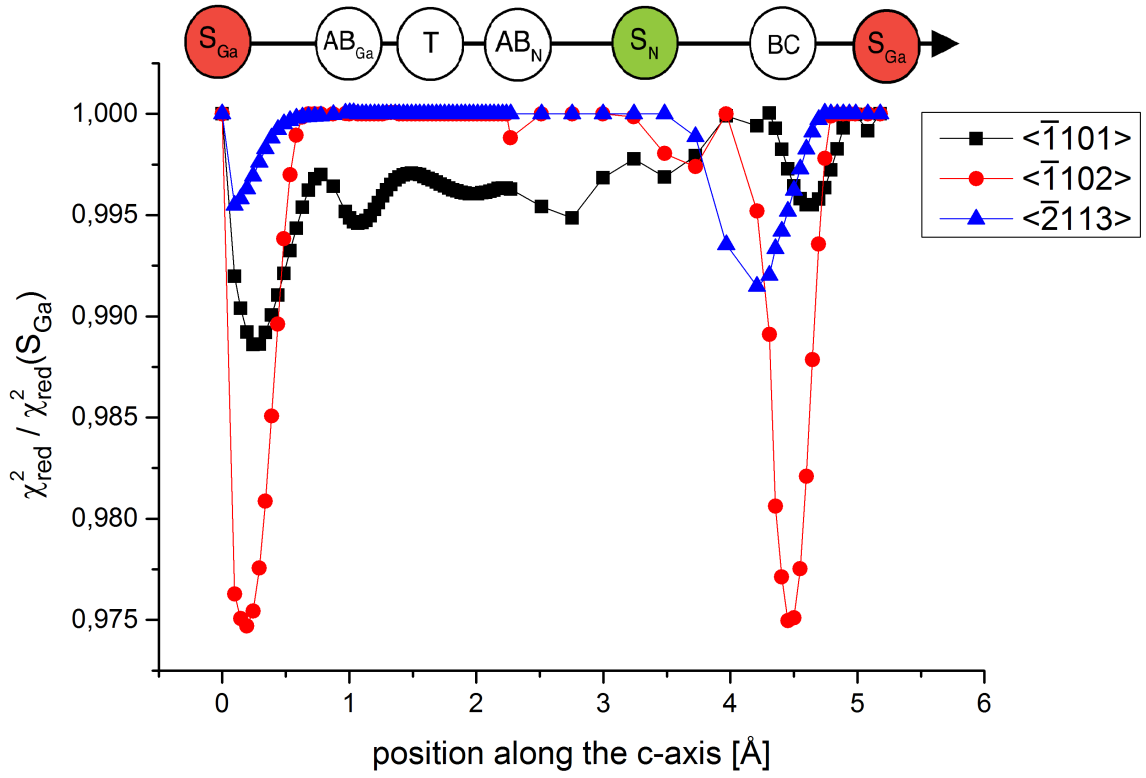


Figure 3.11: Reduced $\chi^2$ values of a two-site fit to the experimental emission yields as seen along the directions $\langle\bar{1}101\rangle$, $\langle\bar{1}102\rangle$ and $\langle\bar{2}113\rangle$ of Fe implanted GaN after a 600° C annealing step. The sites under consideration are $S_{Ga}$,and as second site a high symmetry site or displacements between them along the c-axis. All $\chi^2$ values were normalised to the $\chi^2$ value of $S_{Ga}$. The best fit is achieved with a displacement towards $AB_{Ga}$ but the near BC site also offers a large fit improvement.

### 3.2.5 Comparison 4 samples

In the final analysis the best fit for the lattice location of implanted TM for all four samples was the $S_{Ga}$ site and a displaced $S_{Ga}$ towards the $AB_{Ga}$ site. As in the earlier work by Pereira et al.[71], summarised in section 3.2.1, we attribute the displaced fraction of the implanted TM to the formation of a complex of the TM cation and the nearest neighbour $V_{Ni}^{c}$. The displacement towards the $AB_{Ga}$ site in undoped GaN and GaMnN rather than the BC site is considered to be due to the positive charge state of $V_{Ni}^{c}$. It is quite surprising however, to observe the same displacement towards the $AB_{Ga}$ site rather than the BC site in n-type GaN. Although the donor doping should in principle move the Fermi level close to the CBM, no effect is observed on the displacement compared to the p-type GaN. Moreover, no anion substitution was observed in any of the Mn implanted GaN and (Ga,Mn)N samples. Since anion substitution was observed for Mn implanted GaN in earlier experiments, and was expected to depend on the position of the Fermi level (GaN samples) and the presence of acceptor states ( (Ga,Mn)N sample), the lack of anion substitution in any of these samples points to an underlying issue.

Both the displacement of $Mn_{sub}$ and the lack of anion substitution suggest that we were unable to control the Fermi level, despite the doping. During implantation a large concentration of vacancies is generated, of the order of a few hundreds per implanted ion. While many of these will recombine immediately with other defects, if the concentration of defects is large enough it is possible for them to pin the Fermi-level, overwhelming the effect of the dopants. This effect has also been found in earlier emission channeling experiments studying the lattice site of Fe in silicon at low and high doping.[53][76]. The reason for the higher radiation-sensitivity for these samples is the non-ideal growth conditions required compared to pure GaN. The lower growth temperature necessary for (Ga,Mn)N synthesis, for example, will lead to larger disorder and likely more efficient damage accumulation compared to pure GaN.

Since the position of the Fermi level after implantation is unknown it is unclear whether the results contradict the selection mechanism outlined before. In the future more careful experiments at higher sample temperature and lower fluence during implantation are necessary to minimise the generation of defects and avoid the effect of Fermi-level pinning. Another possibility under investigation is to perform SSRM measurements (as for (Ga,Mn)As above) to determine the electrical character of the samples after implantation. The depth sensitivity of the technique is especially advantageous as the electrical properties will only be affected in the depth-range of implantation.

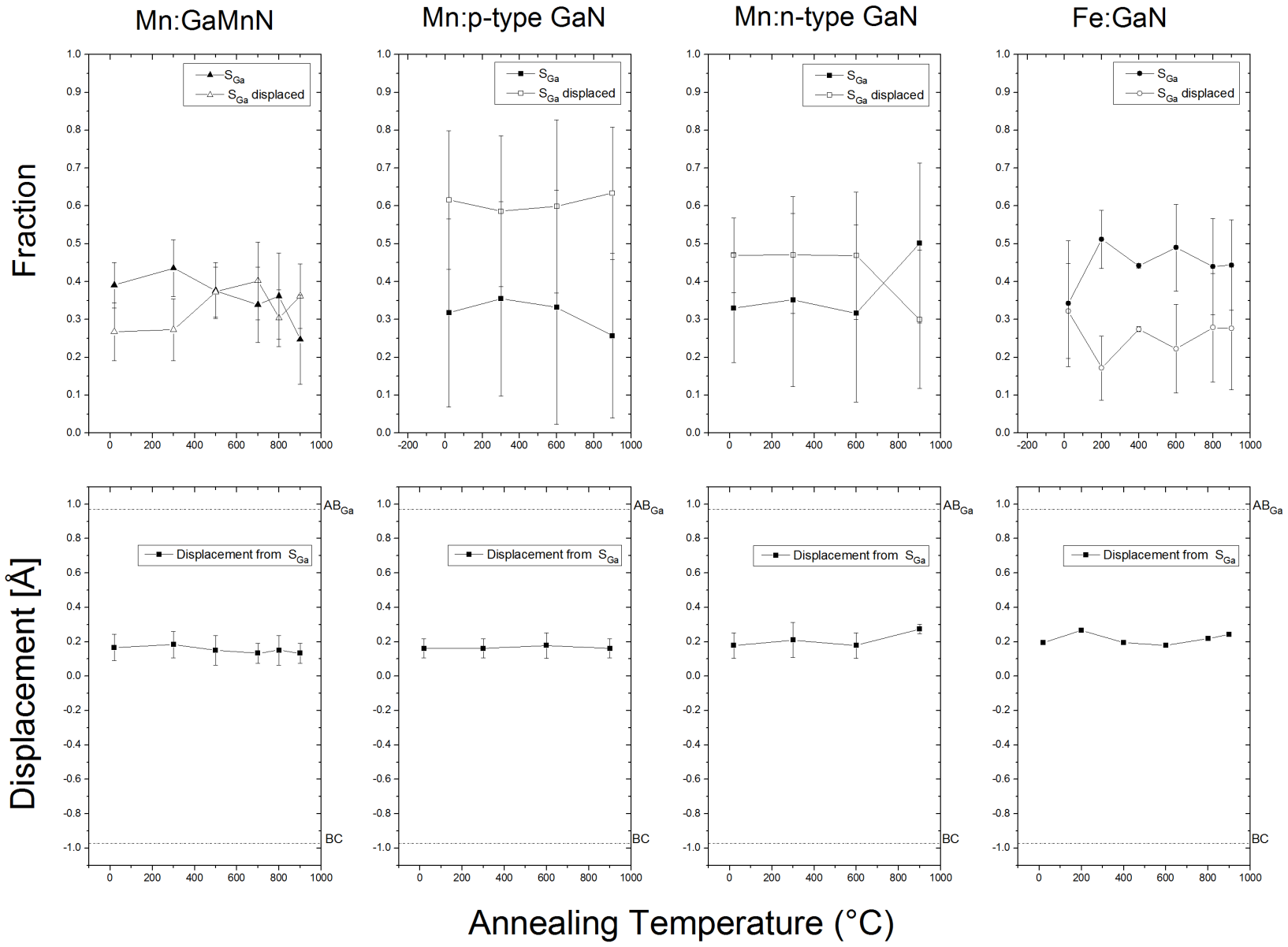


Figure 3.12: In the upper row the occupancy of $S_{Ga}$ and displaced $S_{Ga}$ towards the $Ab_{Ga}$site are shown for Mn implanted GaMnN, p- and n-type GaN and Fe implanted GaN. The graphs in the lower row shows the corresponding displacement along the c-axis.

# Chapter 4

# Conclusion and outlook

The purpose of this work was to study the lattice location of Mn in the dilute magnetic semiconductors (Ga,Mn)As and GaN. In the first part of the thesis the location of Mn in a (Ga,Mn)As thin film of 4 % impurity concentration prepared by ion implantation and pulsed laser melting (II-PLM) was determined. It was shown that the majority of implanted Mn occupies the $S_{Ga}$ position with a minority occupying the $T_{As}$ position, consistent with previous results on molecular beam epitaxy (MBE) samples. However its behaviour under annealing proved to be quite different, with $Mn_{int}$ diffusing already during the first annealing step (25° C -150° C), a diffusion temperature ($T_d$) much lower than what was observed in the MBE samples. This is interpreted to be due to the presence of an internal electric field caused by a non-uniform hole gradient. For substitutional Mn the diffusion temperature of the II-PLM sample was found to be 350° C, in the middle between the diffusion temperatures of the MBE samples. This is consistent with the previously observed monotonous dependence of $T_d$ on the impurity concentration, with samples at higher impurity concentrations having the lowest $T_d$. The direct dependence on the concentration for $Mn_{sub}$ is interpreted to be due to a vacancy-exchange mechanism in a percolation cluster.

Although in GaN cation substitution by Mn ($Mn_{Ga}$) is accepted, there have also been reports of minority anion substitution. This anion fraction could affect the magnetic and electric properties by acting as compensating defect for $Mn_{Ga}$. In this work the lattice location of Mn in (Ga,Mn)N and p- and n-type Gan was found to be a mixture of $Mn_{Ga}$ and displaced $Mn_{Ga}$ towards the $AB_{Ga}$ site. The displaced $Mn_{Ga}$ fraction is proposed to be part of a defect complex with a nitrogen vacancy, created during implantation. The displacement is interpreted to be the result of a repulsive Coulomb interaction with a positively charged nitrogen vacancy as in previous findings. No qualitative difference in the displacement was found between the p- and n-type doped GaN suggesting that

the charge state of the nitrogen vacancy remains positive in both films. As it is known from theoretical studies that for highly n-type doped GaN the nitrogen vacancy should be negatively charged, we expect that in fact the Fermi-level could not be controlled. This would be the result of defects, generated by excessive implantation damage, pinning the Fermi-level in the middle of the bandgap.

To expand on these experiments in the future, scanning spreading resistance microscopy studies are under way to determine the electrical properties of both the GaN and (Ga,Mn)As films. As this technique quantifies the hole concentration over the depth range of the film, it will serve to determine if the electrical field hypothesis for the interstitial diffusion mechanism is correct in the (Ga,Mn)As film. In the GaN films it should serve to determine if indeed the Fermi level was pinned in the range of implantation, negating the effect of doping locally.

# Bibliography


[1] S A Wolf et al. "Spintronics: a spin-based electronics vision for the future." In: *Science (New York, N.Y.)* 294.5546 (Nov. 2001), pp. 1488–95. ISSN: 0036-8075. DOI: 10.1126/science.1065389.

[2] NF Mott. "The electrical conductivity of transition metals". In: *Proceedings of the Royal Society of London. Series A, ...* (1936).

[3] A Fert and IA Campbell. "Two-current conduction in nickel". In: *Physical Review Letters* 21.16 (1968), pp. 15–17.

[4] Igor Žutić, Jaroslav Fabian, and S. Das Sarma. *Spintronics: Fundamentals and applications*. 2004.

[5] H Ohno. "Making Nonmagnetic Semiconductors Ferromagnetic". In: *Science* 281.5379 (Aug. 1998), pp. 951–956. DOI: 10.1126/science.281.5379.951.

[6] J. K. Furdyna. "Diluted magnetic semiconductors". In: *Journal of Applied Physics* 64.4 (1988), R29. ISSN: 00218979. DOI: 10.1063/1.341700.

[7] Sanghoon Lee et al. "Ferromagnetic semiconductor GaMnAs". In: *Materials Today* 12.4 (Apr. 2009), pp. 14–21. ISSN: 13697021. DOI: 10.1016/S1369-7021(09)70109-9.

[8] H Munekata et al. "Diluted magnetic III-V semiconductors". In: *Physical Review Letters* 63.17 (Oct. 1989), pp. 1849–1852. ISSN: 0031-9007. DOI: 10.1103/PhysRevLett.63.1849.

[9] A. Shen et al. "Epitaxy of (Ga, Mn)As, a new diluted magnetic semiconductor based on GaAs". In: *Journal of Crystal Growth* 175-176 (May 1997), pp. 1069–1074. DOI: 10.1016/s0022-0248(96)00967-0.

[10] L. Chen et al. "Low-temperature magnetotransport behaviors of heavily Mn-doped (Ga, Mn)As films with high ferromagnetic transition temperature". In: *Applied Physics Letters* 95.18 (2009), p. 182505. DOI: 10.1063/1.3259821.

[11] T. Dietl. "Zener Model Description of Ferromagnetism in Zinc-Blende Magnetic Semiconductors". In: *Science* 287.February (2000), pp. 1019–1022. ISSN: 00368075. DOI: 10.1126/science.287.5455.1019.

[12] Wiktor Stefanowicz et al. "Structural and paramagnetic properties of dilute Ga 1 - x Mn x N". In: *Physical Review B* 81.23 (June 2010). DOI: 10.1103/physrevb.81.235210.

[13] a. Ney et al. "Anisotropic paramagnetism of Co-doped ZnO epitaxial films". In: *Physical Review B - Condensed Matter and Materials Physics* 81 (2010), pp. 1–10. ISSN: 10980121. DOI: 10.1103/PhysRevB.81.054420.

[14] E. Sarigiannidou et al. "Intrinsic ferromagnetism in wurtzite (Ga,Mn)N semiconductor". In: *Physical Review B* 74 (2006), 041306(R). ISSN: 1098-0121. DOI: 10.1103/PhysRevB.74.041306.

[15] Nitin Samarth. "Ferromagnetic semiconductors: Battle of the bands". In: *Nature Materials* 11.May (2012), pp. 360–361. ISSN: 1476-1122. DOI: 10.1038/nmat3317.

[16] M Dobrowolska et al. "Controlling the Curie temperature in (Ga,Mn)As through location of the Fermi level within the impurity band." In: *Nature materials* 11.5 (May 2012), pp. 444–9. ISSN: 1476-1122. DOI: 10.1038/nmat3250.

[17] Tomasz Dietl and Hideo Ohno. "Dilute ferromagnetic semiconductors: Physics and spintronic structures". In: *Reviews of Modern Physics* 86.1 (Mar. 2014), pp. 187–251. ISSN: 0034-6861. DOI: 10.1103/RevModPhys.86.187.

[18] T. Jungwirth et al. "Prospects for high temperature ferromagnetism in (Ga,Mn)As semiconductors". In: *Physical Review B* 72.16 (Oct. 2005), p. 165204. ISSN: 1098-0121. DOI: 10.1103/PhysRevB.72.165204.

[19] H Kepa et al. "Probing hole-induced ferromagnetic exchange in magnetic semiconductors by inelastic neutron scattering." In: *Physical review letters* 91.August (2003), p. 087205. ISSN: 0031-9007. DOI: 10.1103/PhysRevLett.91.087205.

[20] K Sato, P. H Dederics, and H Katayama-Yoshida. *Curie temperatures of III–V diluted magnetic semiconductors calculated from first principles*. 2007. DOI: 10.1209/epl/i2003-00191-8.

[21] H Akai. "Ferromagnetism and its stability in the diluted magnetic semiconductor (In, Mn) As". In: *Physical review letters* 81 (1998), pp. 3002–3005. ISSN: 0031-9007. DOI: 10.1103/PhysRevLett.81.3002.

[22] Kevin Edmonds, Gerrit van der Laan, and Giancarlo Panaccione. "Electronic structure of (Ga, Mn)As as seen by synchrotron radiation". In: *Semicond. Sci. Technol.* 30.4 (Feb. 2015), p. 043001. DOI: 10.1088/0268-1242/30/4/043001.

[23] M. Wang et al. "Achieving high Curie temperature in (Ga,Mn)As". In: *Applied Physics Letters* 93.2008 (2008), pp. 16–19. ISSN: 00036951. DOI: 10.1063/1.2992200.

[24] K.W. Edmonds, P. Bogusławski, and K.Y. Wang. "Mn Interstitial Diffusion in GaMnAs". In: *Physical Review Letters* 92 (2004), p. 037201. ISSN: 0031-9007. DOI: 10.1103/PhysRevLett.92.037201.

[25] T Jungwirth et al. "Prospects for high temperature ferromagnetism in (Ga, Mn) As semiconductors". In: *Physical Review B* 72 (2005), p. 165204. DOI: 10.1103/PhysRevB.72.165204.

[26] R. Shioda et al. "Local structures of III-V diluted magnetic semiconductors Ga 1 - x Mn x As studied using extended x-ray-absorption fine structure". In: *Physical Review B* 58.3 (July 1998), pp. 1100–1102. DOI: 10.1103/physrevb.58.1100.

[27] R. Bacewicz et al. "Local structure of Mn in (Ga, Mn)As probed by X-ray absorption spectroscopy". In: *Journal of Physics and Chemistry of Solids* 66.11 (Nov. 2005), pp. 2004–2007. DOI: 10.1016/j.jpcs.2005.09.039.

[28] K. Yu et al. *Effect of the location of Mn sites in ferromagnetic Ga1-xMnxAs on its Curie temperature*. Apr. 2002. DOI: 10.1103/PhysRevB.65.201303.

[29] K. Lawniczak-Jablonska et al. "The ratio of interstitial to substitutional site occupation by Mn atoms in GaAs estimated by EXAFS". In: *Radiation Physics and Chemistry* 78.10 (Oct. 2009), S80–S85. DOI: 10.1016/j.radphyschem.2009.03.089.

[30] V. Holý et al. "Density of Mn interstitials in (Ga,Mn)As epitaxial layers determined by anomalous x-ray diffraction". In: *Applied Physics Letters* 97.18 (2010), pp. 4–6. ISSN: 00036951. DOI: 10.1063/1.3514240.

[31] F. Glas et al. "Determination of the Local Concentrations of Mn Interstitials and Antisite Defects in G a M n A s". In: *Phys. Rev. Lett.* 93.8 (Aug. 2004). DOI: 10.1103/physrevlett.93.086107.

[32] V. Baykov, P. Korzhavyi, and B. Johansson. "Diffusion of Interstitial Mn in the Dilute Magnetic Semiconductor (Ga,Mn)As: The Effect of a Charge State". In: *Physical Review Letters* 101.17 (Oct. 2008), p. 177204. ISSN: 0031-9007. DOI: 10.1103/PhysRevLett.101.177204.

[33] L. M. C. Pereira et al. "Direct identification of interstitial Mn in heavily p-type doped GaAs and evidence of its high thermal stability". In: *Applied Physics Letters* 98.20 (2011), p. 201905. ISSN: 00036951. DOI: 10.1063/1.3592568.

[34] L. M. C. Pereira et al. "Stability and diffusion of interstitial and substitutional Mn in GaAs of different doping types". In: *Physical Review B* 86.12 (Sept. 2012), p. 125206. ISSN: 1098-0121. DOI: 10.1103/PhysRevB.86.125206.

[35] T. a. L. Lima et al. "Identification of the interstitial Mn site in ferromagnetic (Ga,Mn)As". In: *Applied Physics Letters* 106.1 (2015), p. 012406. ISSN: 0003-6951. DOI: 10.1063/1.4905556.

[36] S. Strite. "GaN, AlN, and InN: A review". In: *Journal of Vacuum Science & Technology B: Microelectronics and Nanometer Structures* 10.4 (July 1992), p. 1237. DOI: 10.1116/1.585897.

[37] Nikolay Smolentsev et al. "Local atomic structure around Mn ions in GaN:Mn thin films: Quantitative XANES analysis". In: *Physica B: Condensed Matter* 406.14 (July 2011), pp. 2843–2846. DOI: 10.1016/j.physb.2011.04.041.

[38] S. Kuroda et al. "Structural analysis of (Ga,Mn)N epilayers and self-organized dots using MeV ion channeling". In: *Physica Status Solidi (A) Applications and Materials Science* 203.7 (2006), pp. 1724–1728. ISSN: 18626300. DOI: 10.1002/pssa.200565396.

[39] Fumiyoshi Takano et al. "Growth and characterization of Mn-doped cubic-GaN". In: *Physica B: Condensed Matter* 376-377 (Apr. 2006), pp. 658–662. DOI: 10.1016/j.physb.2005.12.166.

[40] L. M. C. Pereira et al. "Evidence of N substitution by Mn in GaN". In: *Physical Review B* 86.19 (Nov. 2012), p. 195202. ISSN: 1098-0121. DOI: 10.1103/PhysRevB.86.195202.

[41] J. Buckeridge et al. "Determination of the Nitrogen Vacancy as a Shallow Compensating Center in GaN Doped with Divalent Metals". In: *Physical Review Letters* 016405.January (2015), pp. 1–5. ISSN: 0031-9007. DOI: 10.1103/PhysRevLett.114.016405.

[42] C. Liu, F. Yun, and H. Morkoç. "Ferromagnetism of ZnO and GaN: A Review". In: *Journal of Materials Science: Materials in Electronics* 16.9 (Sept. 2005), pp. 555–597. DOI: 10.1007/s10854-005-3232-1.

[43] J M D Coey, M Venkatesan, and C B Fitzgerald. "Donor impurity band exchange in dilute ferromagnetic oxides." In: *Nature materials* 4.2 (2005), pp. 173–179. ISSN: 1476-1122. DOI: 10.1038/nmat1310.

[44] a. Bonanni et al. "Experimental probing of exchange interactions between localized spins in the dilute magnetic insulator (Ga,Mn)N". In: *Physical Review B - Condensed Matter and Materials Physics* 84.3 (2011), pp. 1–11. ISSN: 10980121. DOI: 10.1103/PhysRevB.84.035206.

[45] T. Hayashi et al. "(GaMn)As: GaAs-based III-V diluted magnetic semiconductors grown by molecular beam epitaxy". In: *Journal of Crystal Growth* 175-176 (May 1997), pp. 1063–1068. DOI: 10.1016/s0022-0248(96)00937-2.

[46] M. a. Scarpulla et al. "Ferromagnetic Ga[sub 1x]Mn[sub x]As produced by ion implantation and pulsed-laser melting". In: *Applied Physics Letters* 82.8 (2003), p. 1251. ISSN: 00036951. DOI: 10.1063/1.1555260.

[47] Danilo Bürger et al. "Application of pulsed laser annealing to ferromagnetic GaMnAs". In: *Physical Review B* 81.11 (Mar. 2010), p. 115202. ISSN: 1098-0121. DOI: 10.1103/PhysRevB.81.115202.

[48] M. a. Scarpulla et al. "Electrical transport and ferromagnetism in $Ga_{1x}Mn_x$ As synthesized by ion implantation and pulsed-laser melting". In: *Journal of Applied Physics* 103.7 (2008), p. 073913. ISSN: 00218979. DOI: 10.1063/1.2890411.

[49] L. M. C. Pereira. "Structure and magnetism of transition-metal implanted dilute magnetic semiconductors". PhD thesis. KU Leuven, 2011.

[50] H. H. Tan et al. "Ion damage buildup and amorphization processes in AlxGa1-xAs". In: *J. Appl. Phys.* 77.1 (1995), p. 87. DOI: 10.1063/1.359358.

[51] P. Van Duppen. "Isotope Separation On Line and Post Acceleration". In: *The Euroschool Lectures on Physics with Exotic Beams, Vol. II*. Springer Science Business Media, 2006, pp. 37–77. DOI: 10.1007/3-540-33787-3_2.

[52] De Vries B. "Lattice site location of impurities in group III nitrides using emission channeling". PhD thesis. KU Leuven, 2006.

[53] D. J. Silva et al. "Influence of n+] and p+ doping on the lattice sites of implanted Fe in Si". In: *J. Appl. Phys.* 114.10 (2013), p. 103503. DOI: 10.1063/1.4819210.

[54] J. G. Correia, K. Johnston, and U. Wahl. "Nuclear radioactive techniques applied to materials research". In: *Radiochimica Acta* 100.2 (Feb. 2012), pp. 127–137. DOI: 10.1524/ract.2011.1873.

[55] Hans Hofsäss and Gerhard Lindner. "Emission channeling and blocking". In: *Physics Reports* 201.3 (Mar. 1991), pp. 121–183. DOI: 10.1016/0370-1573(91)90121-2.

[56] Ulrich Wahl. In: *Hyperfine Interactions* 129.1/4 (2000), pp. 349–370. DOI: 10.1023/a:1012697429920.

[57] Steven C. Erwin and A. G. Petukhov. "Self-Compensation in Manganese-Doped Ferromagnetic Semiconductors". In: *Phys. Rev. Lett.* 89.22 (Nov. 2002). DOI: 10.1103/physrevlett.89.227201.

[58] T. a. L. Lima. "Local structure and magnetism of (Ga,Mn)As". MA thesis. KU Leuven, 2014.

[59] K. W. Edmonds et al. "Mn Interstitial Diffusion in ( G a , M n ) A s". In: *Phys. Rev. Lett.* 92.3 (Jan. 2004). DOI: 10.1103/physrevlett.92.037201.

[60] Hannes Raebiger, Maria Ganchenkova, and Juhani von Boehm. "Diffusion and clustering of substitutional Mn in (Ga, Mn)As". In: *Applied Physics Letters* 89.1 (2006), p. 012505. DOI: 10.1063/1.2219337.

[61] Robert E. Behringer. "Number of Single, Double, and Triple Clusters in a System Containing Two Types of Atoms". In: *J. Chem. Phys.* 29.3 (1958), p. 537. DOI: 10.1063/1.1744537.

[62] F. Smits. "Formation of Junction Structures by Solid-State Diffusion". In: *Proceedings of the IRE* 46.6 (June 1958), pp. 1049–1061. DOI: 10.1109/jrproc.1958.286843.

[63] L. Horák et al. "Diffusion of Mn interstitials in (Ga,Mn)As epitaxial layers". In: *Physical Review B - Condensed Matter and Materials Physics* 83 (2011), pp. 1–7. ISSN: 10980121. DOI: 10.1103/PhysRevB.83.245209.

[64] O. Proselkov et al. "Thickness dependent magnetic properties of (Ga,Mn)As ultrathin films". In: *Applied Physics Letters* 100.2012 (2012). ISSN: 00036951. DOI: 10.1063/1.4731202.

[65] S Hu. "Nonequilibrium point defects and diffusion in silicon". In: *Materials Science and Engineering: R: Reports* 13 (1994), pp. 105–192. ISSN: 0927796X. DOI: 10.1016/0927-796X(94)90009-4.

[66] D. Mathiot and J. C. Pfister. "Dopant diffusion in silicon: A consistent view involving nonequilibrium defects". In: *Journal of Applied Physics* 55.10 (1984), p. 3518. ISSN: 00218979. DOI: 10.1063/1.332941.

[67] A. Nylandsted Larsen et al. "Heavy doping effects in the diffusion of group IV and V impurities in silicon". In: *Journal of Applied Physics* 73.2 (1993), p. 691. ISSN: 00218979. DOI: 10.1063/1.353324.

[68] Zhihu Sun et al. "Evidence of substitutional Co ion clusters in Zn 1 - x Co x O dilute magnetic semiconductors". In: *Physical Review B* 77.24 (June 2008). DOI: 10.1103/physrevb.77.245208.

[69] J.C. Pivin et al. "Structure and magnetic properties of ZnO films doped with Co, Ni or Mn synthesized by pulsed laser deposition under low and high oxygen partial pressures". In: *Thin Solid Films* 517.2 (Nov. 2008), pp. 916–922. DOI: 10.1016/j.tsf.2008.08.125.

[70] J. A. Sans et al. "Thermal instability of implanted Mn ions in ZnO". In: *J. Appl. Phys.* 107.2 (2010), p. 023507. DOI: 10.1063/1.3275890.

[71] L.M.C. Pereira et al. "Emission channeling studies on transition-metal doped GaN and ZnO: Cation versus anion substitution". In: *Nuclear Instruments and Methods in Physics Research Section B: Beam Interactions with Materials and Atoms* 332 (Aug. 2014), pp. 143–147. DOI: 10.1016/j.nimb.2014.02.048.

[72] Sukit Limpijumnong and Chris Van de Walle. "Diffusivity of native defects in GaN". In: *Physical Review B* 69 (2004), pp. 1–11. ISSN: 1098-0121. DOI: 10.1103/PhysRevB.69.035207.

[73] U. Gerstmann, a. Blumenau, and H. Overhof. "Transition metal defects in group-III nitrides: An ab initio calculation of hyperfine interactions and optical transitions". In: *Physical Review B* 63 (2001), pp. 1–9. ISSN: 0163-1829. DOI: 10.1103/PhysRevB.63.075204.

[74] M. G. Ganchenkova and R. M. Nieminen. "Nitrogen vacancies as major point defects in gallium nitride". In: *Physical Review Letters* 96.May (2006), pp. 1–4. ISSN: 00319007. DOI: 10.1103/PhysRevLett.96.196402.

[75] U. Wahl et al. “Direct evidence for implanted Fe on substitutional Ga sites in GaN”. In: *Applied Physics Letters* 78.21 (2001), pp. 3217–3219. ISSN: 00036951. DOI: 10.1063/1.1372201.

[76] U. Wahl et al. “Lattice sites of implanted Fe in Si”. In: *Physical Review B* 72.1 (July 2005). DOI: 10.1103/physrevb.72.014115.

AFDELING
Straat nr bus
3000 LEUVEN, BEL
tel. + 32 16 00 0
fax + 32 16 00 0
www.kuleuve